 CMC, vol.29, no.3, pp.213-261, 2012

Analysis of Functionally Graded Magneto-Electro-Elastic Composites Using Hybrid/Mixed Finite Elements and Node-Wise Material Properties

Peter L. Bishay[1], Jan Sladek[2], Vladimir Sladek[2] and Satya N. Atluri[1]

Abstract: A new class of hybrid/mixed finite elements, denoted "HMFEM-C", has been developed for modeling magneto-electro-elastic (MEE) materials. These elements are based on assuming independent strain-fields, electric and magnetic fields, and collocating them with the strain-fields, electric and magnetic fields derived from the primal variables (mechanical displacements, electric and magnetic potentials) at some cleverly chosen points inside each element. The newly developed elements show significantly higher accuracy than the primal elements for the electric, magnetic as well as the mechanical variables. HMFEM-C is invariant through the use of the element-fixed local orthogonal base vectors, and is stable since it is not derived from a multi-field variational principle; hence it completely avoids LBB conditions that govern the stability of hybrid/mixed elements. In this paper, node-wise material properties are used in order to better simulate the spatial material grading of the functionally graded materials (FGM). A computer code was developed, validated and used to calculate the three magnetoelectric (ME) voltage coefficients for piezoelectric-piezomagnetic (PE-PM) composites, namely, the out-of-plane, transverse and in-plane ME voltage coefficients. The effects of the piezoelectric phase volume fraction as well as the mechanical boundary conditions and loadings on the ME voltage coefficients are investigated. Also, the effects of grading functions in PE-PM composites with functionally graded layers, as well as single-layered functionally graded magneto-electro-elastic materials, on the three ME voltage coefficients are presented.

Keywords: Collocation; piezoelectric; functionally graded materials; magneto-electric (ME) voltage coefficient.

[1] Center for Aerospace Research & Education, University of California, Irvine, CA, USA.
[2] Institute of Construction and Architecture, Slovak Academy of Sciences, Slovakia.

1 Introduction

Bringing ferroelectricity and magnetism together in one material proved to be a difficult problem, as these phenomena turned out to be mutually exclusive [Schmid (1994); Hill (2000); Khomskii (2001); Lines and Glass (2001); Van Aken *et al.* (2004); Eerenstein *et al.* (2006)]. Furthermore, it was found that the simultaneous presence of electric and magnetic dipoles does not guarantee strong coupling between the two, as microscopic mechanisms of ferroelectricity and magnetism are quite different and do not strongly interfere with each other [Cheong and Mostovoy (2007)]. However, designing composites made up of pure piezoelectric and pure piezomagnetic phases can lead to higher magnetoelectric (ME) coupling in the whole structure. Hence, the strong magnetoelectric effect is a byproduct property of the composite structure, which is absent in the individual phases [Ryu *et al.* (2002)]. Remarkably larger magnetoelectric effect is observed for composites than for either composite constituents in [Nan (1994); Feng and Su (2006)] and higher piezoelectric strain modulus d_{31} is found in piezo-composites than in the constituents [Smith and Shaulov (1985) and Shaulov *et al.* (1989)]. Also, the numerical results by Dunn (1993) showed that the effective thermal expansion coefficients of composites could significantly exceed those of the matrix and the fiber phases.

Strong megnetoelectric coupling can be utilized in energy conversion between the magnetic and electric fields and smart sensors and transducers [Wang *et al.* (2005)]. Due to the hysteretic nature of the ME effect, the multiferroic composites may find applications in ME memory elements and memory devices. Further applications include magnetic field sensors and magnetically controlled opto-electronic devices. The transduction properties of the ME effect can also be employed in ME recording heads and electromagnetic pick-ups. Historical perspectives, status and future of multiferroic magnetoelectric composites are given in a review paper [Nan *et al.* (2008)].

Magnetoelectric coupling can be greatly enhanced by using laminated double, triple or multilayer piezoelectric-piezomagnetic composites. The magnetoelectric (ME) coefficients are defined as the ratio between the electrical (magnetic) field output over the magnetic (electrical) field input. For a bi-layer piezoelectric-piezomagnetic (PE-PM) composite, an applied magnetic field induces strain in the piezomagnetic constituent which is passed on to the piezoelectric constituent, where it induces an electric polarization. In turn, an applied magnetic field induces polarization via the mechanical coupling between the constituents. A strong ME effect has been recently observed by [Pan and Wang (2009)] in artificially fabricated multiferroic composites. It has been shown that the ME response of the laminated composites is determined by four major aspects: (i) the magnetic, electrical and mechanical co-

efficients of the constituents; (ii) the respective thickness and number of the piezoelectric and magnetostrictive layers; (iii) the type of boundary constituents; (iv) the orientation of the constituents and of the applied electric or magnetic fields. The influence of the thickness ratio for piezomagnetic and piezoelectric layers h_m/h_e on the ME effect was investigated in other papers too [Shastry *et al.* (2004); Laletin *et al.* (2008); Zhai *et al.* (2004)]. The two-dimensional behavior of laminated magneto-electro-elastic plates is investigated by Heyliger *et al.* (2004) for two specific geometries: laminates under conditions of cylindrical bending and homogeneous plates under traction-free conditions. Sladek *et al.* (2012 a, b) used the MLPG method to analyze the effects of boundary conditions and layer thickness on multiferroic composites and functionally graded multiferroic composites. In functionally graded materials (FGMs) the volume fraction of constituents varies in a predominant direction [Miyamoto *et al.* (1999)]. Due to their grading feature, FGMs could have many interesting applications in various piezoelectric devices [Carbonari *et al.* (2007), (2009), (2010)].

Solving the governing equations of piezoelectricity and magneto-electro-elasticity analytically is only limited to few simple problems such as simply-supported beams and plates. Modeling piezoelectric materials using the finite element method was one of the most active research topics in the last two decades. Benjeddou (2000) presented a survey for all the elements developed to model piezoelectric materials until year 2000. He presented the approximation method and the degrees of freedom for all the developed element types for the different structural members. Taking the mechanical displacements and electric potential only as the independent variables, irreducible finite elements are developed (irreducible in the sense that the number of field variables cannot be further reduced). Irreducible elements for the different structural members were developed. For example, Irreducible 2D piezoelectric solid elements were presented by Kagawa and Yarnahuchi (1974) and by Naillon *et al.* (1983); while irreducible 3D piezoelectric solid elements were presented by Lerch (1990) and by Hossack and Hayward (1991). Piezoelectric plate elements and laminated composites with embedded piezoelectric plates were developed by Hwang and Park (1993), Heyliger *et al.* (1994), Kim *et al.* (1997) and by Saravanos *et al.* (1997). Tzou and Tseng (1990) also developed piezoelectric plate element by adding incompatible modes to the 3D hexahedron solid element. Piezoelectric shell elements and laminated shells can be found in [Tzou (1993); Tzou and Ye (1996)].

However, since the irreducible piezoelectric elements are similar to the displacement-based structural elements in being too stiff, very sensitive to mesh distortion and aspect ratio, and suffer from the locking phenomena, hybrid/mixed piezoelectric elements were developed to overcome these disadvantages. Not only the mechan-

ical displacements and the electric potential are the independent variables in the hybrid/mixed elements, but also other fields such as the stress field or the electric displacement are independently assumed. In [Ghandi, and Hagood (1997)], the additionally assumed field was the electric displacement while in [Sze and Pan (1999)], it was the mechanical stress. Both elements were superior to the irreducible elements. Also the bubble/incompatible displacement modes method was used to improve the performance of the irreducible elements in [Tzou and Tseng (1990); Tzou (1993) and others].

In this paper, hybrid/mixed finite elements are used to model piezoelectric-piezomagnetic (PE-PM) composites and functionally graded magneto-electro-elastic-(MEE) composites. The HMFEM elements used here, are denoted "HMFEM-C", since it is based on independently assuming the secondary fields (strain, electric and magnetic fields) and enforcing the compatibility between these fields and the secondary fields derived from the primal fields (mechanical displacements, electric and magnetic potentials) by a method of collocation at cleverly chosen points. The "HMFEM-C" elements are the extension of the HMFEM-2 elements presented in [Dong and Atluri (2011); Bishay and Atluri (2012)] for elasticity problems, and which proved to be superior in performance over the primal elements especially when the structure is loaded in bending or shear.

The current work uses nodal-defined material properties which are more suitable to deal with FGM as they provide smooth grading of the material properties and prevent jumps in the material properties between elements that are encountered when using element-wise material properties. The advantage of using these nodal-defined material properties can be more significant in the case of higher-order elements which are able to model quadratic variations especially when the grading function is non-linear. We investigate PE-PM composites with functionally graded layers as well as single-layer functionally graded MEE material with pure piezomagnetic properties on its bottom surface and pure piezoelectric properties on its top surface. Along the thickness of the functionally graded layer the material properties are continuously varying. Both pure constituents have a vanishing ME coefficient. The influences of various mechanical boundary conditions and loadings as well as volume ratio of piezoelectric and piezomagnetic constituents on the ME coefficient are investigated in several numerical experiments.

The rest of the paper is organized as follows; in section 2, the governing equations of magneto-electro-elasticity will be introduced, with the finite element formulations for the primal elements and the new hybrid/mixed elements being presented in section 3 together with the nodal-defined material properties technique. Section 4 is devoted for defining the three ME voltage coefficients and the magnetic and electric BCs used to model these three modes. Section 5 begins with the computer

code validation through the patch test and cantilevered MEE beam problem with end shear load, then analysis of bi-layered PE-PM composites, bi-layered PE-PM composites with functionally graded layers and single-layer functionally graded magneto-electro-elastic material are presented. The influence of the boundary conditions, loadings, and grading is illustrated. Conclusions are summarized in section 6.

2 Governing equations

Adopting matrix and vector notation and denoting $\mathbf{u}$, $\boldsymbol{\varepsilon}$ and $\boldsymbol{\sigma}$ as the vectors of the mechanical displacement, strain and stress fields, φ, $\mathbf{E}$ and $\mathbf{D}$ as the electric potential, intensity of electric field and electric displacement vectors, and ψ, $\mathbf{H}$ and $\mathbf{B}$ as the magnetic potential, intensity of magnetic field and magnetic induction (or flux density) vectors, we have:

Stress equilibrium equations:

$$\boldsymbol{\partial}_{\mathbf{u}}^{T}\boldsymbol{\sigma}+\overline{\mathbf{b}}=\mathbf{0};\quad \boldsymbol{\sigma}=\boldsymbol{\sigma}^{T}\ \text{ in } \Omega \tag{1}$$

Charge conservation (Maxwell's) equation:

$$\boldsymbol{\partial}_{\mathbf{e}}^{T}\mathbf{D}-\overline{\rho_f}=0 \qquad \text{in } \Omega \tag{2}$$

Maxwell's equation for magnetism:

$$\boldsymbol{\partial}_{\mathbf{m}}^{T}\mathbf{B}=0 \qquad \text{in } \Omega \tag{3}$$

where Ω is the problem domain, $\overline{\mathbf{b}}$ is the body force, and $\overline{\rho_f}$ is the electric free charge density. Note that the right hand-side of eq. (3) is zero because magnetic free charges do not exist in nature.

Strain-displacement equations:

$$\boldsymbol{\varepsilon}=\boldsymbol{\partial}_{\mathbf{u}}\mathbf{u} \tag{4}$$

Electric field- electric potential equations:

$$\mathbf{E}=-\boldsymbol{\partial}_{\mathbf{e}}\varphi \tag{5}$$

Magnetic field- magnetic potential equations:

$$\mathbf{H}=-\boldsymbol{\partial}_{\mathbf{m}}\psi \tag{6}$$

where

$$\boldsymbol{\partial}_{\mathbf{u}} = \begin{bmatrix} \frac{\partial}{\partial x_1} & 0 & 0 & \frac{\partial}{\partial x_2} & 0 & \frac{\partial}{\partial x_3} \\ 0 & \frac{\partial}{\partial x_2} & 0 & \frac{\partial}{\partial x_1} & \frac{\partial}{\partial x_3} & 0 \\ 0 & 0 & \frac{\partial}{\partial x_3} & 0 & \frac{\partial}{\partial x_2} & \frac{\partial}{\partial x_1} \end{bmatrix}^T \quad \boldsymbol{\partial}_{\mathbf{e}} = \boldsymbol{\partial}_{\mathbf{m}} = \begin{bmatrix} \frac{\partial}{\partial x_1} & \frac{\partial}{\partial x_2} & \frac{\partial}{\partial x_3} \end{bmatrix}^T$$

This representation of electric and magnetic fields (eqs. (5) and (6)), as gradients of the electric and magnetic potentials respectively, guarantees the satisfaction of the other two Maxwell's equations ($\nabla \times \mathbf{E} = \mathbf{0}$ and $\nabla \times \mathbf{H} = \mathbf{0}$).

Constitutive laws for magneto-electro-elastic materials:

$$\begin{Bmatrix} \boldsymbol{\sigma} \\ \mathbf{D} \\ \mathbf{B} \end{Bmatrix} = \begin{bmatrix} \mathbf{C} & \mathbf{e}^T & \mathbf{d}^T \\ \mathbf{e} & -\mathbf{h} & -\mathbf{g}^T \\ \mathbf{d} & -\mathbf{g} & -\boldsymbol{\mu} \end{bmatrix} \begin{Bmatrix} \boldsymbol{\varepsilon} \\ -\mathbf{E} \\ -\mathbf{H} \end{Bmatrix} \tag{7}$$

where $\mathbf{C}$ is the elastic stiffness, $\mathbf{h}$ and $\boldsymbol{\mu}$ are the dielectric and magnetic permeability coefficients, respectively, and $\mathbf{e}$, $\mathbf{d}$ and $\mathbf{g}$ are the piezoelectric, piezomagnetic and magnetoelectric material coefficients, respectively.

A pure piezoelectric or piezomagnetic material can be considered as a special case of the general magneto-electro-elastic material described by eq. (7). For a layered PE/PM composite where each layer is either piezoelectric (PE) or piezomagnetic (PM), the constitutive law is reduced to:

$$\begin{Bmatrix} \boldsymbol{\sigma} \\ \mathbf{D} \\ \mathbf{B} \end{Bmatrix} = \begin{bmatrix} \mathbf{C} & \mathbf{e}^T & \mathbf{0} \\ \mathbf{e} & -\mathbf{h} & \mathbf{0} \\ \mathbf{0} & \mathbf{0} & -\boldsymbol{\mu} \end{bmatrix} \begin{Bmatrix} \boldsymbol{\varepsilon} \\ -\mathbf{E} \\ -\mathbf{H} \end{Bmatrix} \text{ for PE layers;} \tag{8}$$

$$\begin{Bmatrix} \boldsymbol{\sigma} \\ \mathbf{D} \\ \mathbf{B} \end{Bmatrix} = \begin{bmatrix} \mathbf{C} & \mathbf{0} & \mathbf{d}^T \\ \mathbf{0} & -\mathbf{h} & \mathbf{0} \\ \mathbf{d} & \mathbf{0} & -\boldsymbol{\mu} \end{bmatrix} \begin{Bmatrix} \boldsymbol{\varepsilon} \\ -\mathbf{E} \\ -\mathbf{H} \end{Bmatrix} \text{ for PM layers.} \tag{9}$$

The SI units of the mentioned fields are as follows: stress $\boldsymbol{\sigma}$ (Pa or N/m^2), strain $\boldsymbol{\varepsilon}$ (no unit or m/m), electric displacement $\mathbf{D}$ (C/m^2), intensity of electric field $\mathbf{E}$ (V/m or N/C), magnetic induction $\mathbf{B}$ (N/Am) and intensity of magnetic field $\mathbf{H}$ (A/m). The SI units of the material matrices are: material elastic stiffness matrix $\mathbf{C}$ (Pa or N/m^2), piezoelectric matrix $\mathbf{e}$ (C/m^2), piezomagnetic matrix $\mathbf{d}$ (N/Am), dielectric matrix $\mathbf{h}$ (C/Vm), magnetoelectric matrix $\mathbf{g}$ (Ns/VC), and magnetic permeability matrix $\boldsymbol{\mu}$ (Ns^2/C^2).

The boundary conditions are:

Mechanical natural (traction) boundary conditions:

$$\mathbf{n}_{\boldsymbol{\sigma}} \boldsymbol{\sigma} = \bar{\mathbf{t}} \quad \text{at } S_t \tag{10}$$

Mechanical essential (displacement) boundary conditions:

$$\mathbf{u} = \bar{\mathbf{u}} \quad \text{at } S_u, \tag{11}$$

Electric natural boundary conditions:

$$\mathbf{n_e D} = \bar{Q} \quad \text{at } S_Q \tag{12}$$

Electric essential boundary conditions:

$$\varphi = \bar{\varphi} \quad \text{at } S_\varphi, \tag{13}$$

Magnetic natural boundary conditions:

$$\mathbf{n_m B} = 0 \quad \text{at } S_B \tag{14}$$

Magnetic essential boundary conditions:

$$\psi = \bar{\psi} \quad \text{at } S_\psi, \tag{15}$$

where $\mathbf{n}_{\boldsymbol{\sigma}} = \begin{bmatrix} n_x & 0 & 0 & n_y & 0 & n_z \\ 0 & n_y & 0 & n_x & n_z & 0 \\ 0 & 0 & n_z & 0 & n_y & n_x \end{bmatrix}$ and $\mathbf{n_e} = \mathbf{n_m} = \begin{bmatrix} n_x & n_y & n_z \end{bmatrix}$,

and $\bar{\mathbf{t}}$ is the boundary traction vector, $\bar{Q}$ is the specified surface density of free charge. n_x, n_y and n_z, the three components of $\mathbf{n}_{\boldsymbol{\sigma}}$, $\mathbf{n_e}$ and $\mathbf{n_m}$, are the components of the unit outward normal to the boundaries S_t, S_Q or S_B. $\bar{\mathbf{u}}$ is the specified mechanical displacement vector at the boundary S_u, $\bar{\varphi}$ is the specified electric potential at the boundary S_φ, and $\bar{\psi}$ is the specified magnetic potential at the boundary S_ψ.

When dividing the whole domain of the body into subdomains, the following conditions should also be satisfied at each subdomain interface S_m:

Mechanical (displacement) compatibility at each inter-subdomain boundary:

$$\mathbf{u}^+ = \mathbf{u}^- \quad \text{at } S_m \tag{16}$$

Mechanical (traction) reciprocity condition at each inter-subdomain boundary:

$$(\mathbf{n}_{\boldsymbol{\sigma}}\boldsymbol{\sigma})^+ + (\mathbf{n}_{\boldsymbol{\sigma}}\boldsymbol{\sigma})^- = 0 \quad \text{at } S_m \tag{17}$$

Electric potential compatibility at each inter-subdomain boundary:

$$\varphi^+ = \varphi^- \quad \text{at } S_m \tag{18}$$

Electric reciprocity condition at each inter-subdomain boundary:

$$(\mathbf{n_e D})^+ + (\mathbf{n_e D})^- = 0 \quad \text{at } S_m \tag{19}$$

Magnetic potential compatibility at each inter-subdomain boundary:

$$\psi^+ = \psi^- \quad \text{at } S_m \tag{20}$$

Magnetic reciprocity condition at each inter-subdomain boundary:

$$(\mathbf{n_m B})^+ + (\mathbf{n_m B})^- = 0 \quad \text{at } S_m \tag{21}$$

2.1 Constitutive law with plane stress and plane strain assumptions

Eq. (7) for hexagonal crystal poled in the 3-direction can be expanded as:

$$\begin{Bmatrix} \sigma_1 \\ \sigma_2 \\ \sigma_3 \\ \sigma_4 \\ \sigma_5 \\ \sigma_6 \\ D_1 \\ D_2 \\ D_3 \\ B_1 \\ B_2 \\ B_3 \end{Bmatrix} = \begin{bmatrix} C_{11} & C_{12} & C_{13} & 0 & 0 & 0 & 0 & 0 & -e_{31} & 0 & 0 & -d_{31} \\ C_{12} & C_{11} & C_{13} & 0 & 0 & 0 & 0 & 0 & -e_{31} & 0 & 0 & -d_{31} \\ C_{13} & C_{13} & C_{33} & 0 & 0 & 0 & 0 & 0 & -e_{33} & 0 & 0 & -d_{33} \\ 0 & 0 & 0 & C_{44} & 0 & 0 & 0 & -e_{15} & 0 & 0 & -d_{15} & 0 \\ 0 & 0 & 0 & 0 & C_{44} & 0 & -e_{15} & 0 & 0 & -d_{15} & 0 & 0 \\ 0 & 0 & 0 & 0 & 0 & C_{66} & 0 & 0 & 0 & 0 & 0 & 0 \\ 0 & 0 & 0 & 0 & e_{15} & 0 & h_{11} & 0 & 0 & g_{11} & 0 & 0 \\ 0 & 0 & 0 & e_{15} & 0 & 0 & 0 & h_{11} & 0 & 0 & g_{11} & 0 \\ e_{31} & e_{31} & e_{33} & 0 & 0 & 0 & 0 & 0 & h_{33} & 0 & 0 & g_{33} \\ 0 & 0 & 0 & 0 & d_{15} & 0 & g_{11} & 0 & 0 & \mu_{11} & 0 & 0 \\ 0 & 0 & 0 & d_{15} & 0 & 0 & 0 & g_{11} & 0 & 0 & \mu_{11} & 0 \\ d_{31} & d_{31} & d_{33} & 0 & 0 & 0 & 0 & 0 & g_{33} & 0 & 0 & \mu_{33} \end{bmatrix} \begin{Bmatrix} \varepsilon_1 \\ \varepsilon_2 \\ \varepsilon_3 \\ \varepsilon_4 \\ \varepsilon_5 \\ \varepsilon_6 \\ E_1 \\ E_2 \\ E_3 \\ H_1 \\ H_2 \\ H_3 \end{Bmatrix} \tag{22}$$

with $C_{66} = \frac{C_{11}-C_{12}}{2}$.

If the considered body is very thin in the 2-direction (plane stress case), we can use the following assumptions:

$$\sigma_2 = \sigma_4 = \sigma_6 = 0\,, \quad D_2 = B_2 = 0 \tag{23}$$

Using $\sigma_2 = 0$ assumption, we can express ε_2 as:

$$\varepsilon_2 = \frac{-C_{12}\varepsilon_1 - C_{13}\varepsilon_3 + e_{31}E_3 + d_{31}H_3}{C_{11}} \tag{24}$$

Substituting this into eq. (22) we get the constitutive equation for plane stress problems:

$$\begin{Bmatrix} \sigma_1 \\ \sigma_3 \\ \sigma_5 \\ D_1 \\ D_3 \\ B_1 \\ B_3 \end{Bmatrix} = \begin{bmatrix} \bar{C}_{11} & \bar{C}_{13} & 0 & 0 & -\bar{e}_{31} & 0 & -\bar{d}_{31} \\ \bar{C}_{13} & \bar{C}_{33} & 0 & 0 & -\bar{e}_{33} & 0 & -\bar{d}_{33} \\ 0 & 0 & \bar{C}_{44} & -\bar{e}_{15} & 0 & -\bar{d}_{15} & 0 \\ 0 & 0 & \bar{e}_{15} & \bar{h}_{11} & 0 & \bar{g}_{11} & 0 \\ \bar{e}_{31} & \bar{e}_{33} & 0 & 0 & \bar{h}_{33} & 0 & \bar{g}_{33} \\ 0 & 0 & \bar{d}_{15} & \bar{g}_{11} & 0 & \bar{\mu}_{11} & 0 \\ \bar{d}_{31} & \bar{d}_{33} & 0 & 0 & \bar{g}_{33} & 0 & \bar{\mu}_{33} \end{bmatrix} \begin{Bmatrix} \varepsilon_1 \\ \varepsilon_3 \\ \varepsilon_5 \\ E_1 \\ E_3 \\ H_1 \\ H_3 \end{Bmatrix} \tag{25}$$

where

$$\bar{C}_{11} = \frac{C_{11}^2 - C_{12}^2}{C_{11}}, \quad \bar{C}_{13} = \frac{C_{13}\,(C_{11} - C_{12})}{C_{11}}, \quad \bar{C}_{33} = \frac{C_{11}C_{33} - C_{13}^2}{C_{11}}, \quad \bar{C}_{44} = C_{44},$$

$$\bar{e}_{31} = \frac{e_{31}\,(C_{11} - C_{12})}{C_{11}}, \quad \bar{e}_{33} = \frac{C_{11}e_{33} - C_{13}e_{31}}{C_{11}}, \quad \bar{e}_{15} = e_{15},$$

$$\bar{d}_{31} = \frac{d_{31}\,(C_{11} - C_{12})}{C_{11}}, \quad \bar{d}_{33} = \frac{C_{11}d_{33} - C_{13}d_{31}}{C_{11}}, \quad \bar{d}_{15} = d_{15},$$

$$\bar{h}_{11} = h_{11}, \quad \bar{h}_{33} = \frac{C_{11}h_{33} + e_{31}^2}{C_{11}},$$

$$\bar{\mu}_{11} = \mu_{11}, \quad \bar{\mu}_{33} = \frac{C_{11}\mu_{33} + d_{31}^2}{C_{11}}, \quad \bar{g}_{11} = g_{11}, \quad \bar{g}_{33} = \frac{C_{11}g_{33} + e_{31}d_{31}}{C_{11}}$$

If the body is very long (infinite) in the 2 - direction (plane strain case), then we have the assumptions:

$$\varepsilon_2 = \varepsilon_4 = \varepsilon_6 = 0\,, \quad E_2 = H_2 = 0 \tag{26}$$

Substituting this directly into eq. (22) we get the constitutive equation for plane strain problems:

$$\begin{Bmatrix} \sigma_1 \\ \sigma_3 \\ \sigma_5 \\ D_1 \\ D_3 \\ B_1 \\ B_3 \end{Bmatrix} = \begin{bmatrix} C_{11} & C_{13} & 0 & 0 & -e_{31} & 0 & -d_{31} \\ C_{13} & C_{33} & 0 & 0 & -e_{33} & 0 & -d_{33} \\ 0 & 0 & C_{44} & -e_{15} & 0 & -d_{15} & 0 \\ 0 & 0 & e_{15} & h_{11} & 0 & g_{11} & 0 \\ e_{31} & e_{33} & 0 & 0 & h_{33} & 0 & g_{33} \\ 0 & 0 & d_{15} & g_{11} & 0 & \mu_{11} & 0 \\ d_{31} & d_{33} & 0 & 0 & g_{33} & 0 & \mu_{33} \end{bmatrix} \begin{Bmatrix} \varepsilon_1 \\ \varepsilon_3 \\ \varepsilon_5 \\ E_1 \\ E_3 \\ H_1 \\ H_3 \end{Bmatrix} \tag{27}$$

3 Finite element modeling of Magneto-Electro-Elastic (MEE) materials

The formulation derived in this section for magneto-electro-elasticity can be directly reduced to piezoelectricity or piezomagnetism by dropping the magnetic or the electric variables, respectively.

The most general variational principle that includes all the nine assumed field variables (stress, strain, displacements, electric displacement, intensity of electric field,

electric potential, magnetic induction, intensity of magnetic field and magnetic potential) for magneto-electro-elastic materials has the form:

$$
\begin{aligned}
&\Pi(\boldsymbol{\sigma},\mathbf{D},\mathbf{B},\boldsymbol{\varepsilon},\mathbf{E},\mathbf{H},\mathbf{u},\varphi,\psi) = \\
&\int_{\Omega}\left[\frac{1}{2}\begin{Bmatrix}\boldsymbol{\varepsilon}\\ -\mathbf{E}\\ -\mathbf{H}\end{Bmatrix}^{T}\begin{bmatrix}\mathbf{C} & \mathbf{e}^{T} & \mathbf{d}^{T}\\ \mathbf{e} & -\mathbf{h} & -\mathbf{g}^{T}\\ \mathbf{d} & -\mathbf{g} & -\boldsymbol{\mu}\end{bmatrix}\begin{Bmatrix}\boldsymbol{\varepsilon}\\ -\mathbf{E}\\ -\mathbf{H}\end{Bmatrix}\right.\\
&\left.-\begin{Bmatrix}\boldsymbol{\sigma}\\ \mathbf{D}\\ \mathbf{B}\end{Bmatrix}^{T}\left(\begin{Bmatrix}\boldsymbol{\varepsilon}\\ -\mathbf{E}\\ -\mathbf{H}\end{Bmatrix}-\begin{Bmatrix}\partial_{\mathbf{u}}\mathbf{u}\\ \partial_{\mathbf{e}}\varphi\\ \partial_{\mathbf{m}}\psi\end{Bmatrix}\right)-\bar{\mathbf{b}}^{T}\mathbf{u}+\overline{\rho_f}\varphi\right]d\Omega\\
&-\int_{S_t}\bar{\mathbf{t}}^{T}\mathbf{u}ds-\int_{S_Q}\bar{Q}\varphi ds-\int_{S_u}(\mathbf{n}_{\boldsymbol{\sigma}}\boldsymbol{\sigma})^{T}(\mathbf{u}-\bar{\mathbf{u}})ds-\int_{S_\varphi}(\mathbf{n}_{\mathbf{e}}\mathbf{D})^{T}(\varphi-\bar{\varphi})ds\\
&\qquad\qquad-\int_{S_\psi}(\mathbf{n}_{\mathbf{m}}\mathbf{B})^{T}(\psi-\bar{\psi})ds \qquad (28)
\end{aligned}
$$

This is the extension of Hu-Washizu principle used in elasticity [see Atluri (1975); Atluri *et al.* (1983); Tang *et al.* (1984)].

The variation of the functional Π gives:

$$
\begin{aligned}
\delta\Pi = \int_{\Omega}&\left[\begin{Bmatrix}\delta\boldsymbol{\varepsilon}\\ -\delta\mathbf{E}\\ -\delta\mathbf{H}\end{Bmatrix}^{T}\left(\begin{bmatrix}\mathbf{C} & \mathbf{e}^{T} & \mathbf{d}^{T}\\ \mathbf{e} & -\mathbf{h} & -\mathbf{g}^{T}\\ \mathbf{d} & -\mathbf{g} & -\boldsymbol{\mu}\end{bmatrix}\begin{Bmatrix}\delta\boldsymbol{\varepsilon}\\ -\delta\mathbf{E}\\ -\delta\mathbf{H}\end{Bmatrix}-\begin{Bmatrix}\boldsymbol{\sigma}\\ \mathbf{D}\\ \mathbf{B}\end{Bmatrix}^{T}\right)\right.\\
&\left.-\begin{Bmatrix}\delta\boldsymbol{\sigma}\\ \delta\mathbf{D}\\ \delta\mathbf{B}\end{Bmatrix}^{T}\left(\begin{Bmatrix}\boldsymbol{\varepsilon}\\ -\mathbf{E}\\ -\mathbf{H}\end{Bmatrix}-\begin{Bmatrix}\partial_{\mathbf{u}}\mathbf{u}\\ \partial_{\mathbf{e}}\varphi\\ \partial_{\mathbf{m}}\psi\end{Bmatrix}\right)-\begin{Bmatrix}\delta\mathbf{u}\\ \delta\varphi\\ \delta\psi\end{Bmatrix}^{T}\begin{Bmatrix}\partial_{\mathbf{u}}^{T}\boldsymbol{\sigma}+\bar{\mathbf{b}}\\ \partial_{\mathbf{e}}^{T}\mathbf{D}-\overline{\rho_f}\\ \partial_{\mathbf{m}}^{T}\mathbf{B}\end{Bmatrix}\right]d\Omega\\
&-\int_{S_t}(\mathbf{n}_{\boldsymbol{\sigma}}\boldsymbol{\sigma}-\bar{\mathbf{t}})^{T}\delta\mathbf{u}ds-\int_{S_Q}(\mathbf{n}_{\mathbf{e}}\mathbf{D}-\bar{Q})\delta\varphi ds-\int_{S_B}(\mathbf{n}_{\mathbf{m}}\mathbf{B})\delta\psi ds\\
&-\int_{S_u}(\mathbf{n}_{\boldsymbol{\sigma}}\delta\boldsymbol{\sigma})^{T}(\mathbf{u}-\bar{\mathbf{u}})ds-\int_{S_\varphi}(\mathbf{n}_{\mathbf{e}}\delta\mathbf{D})^{T}(\varphi-\bar{\varphi})ds-\int_{S_\psi}(\mathbf{n}_{\mathbf{m}}\delta\mathbf{B})^{T}(\psi-\bar{\psi})ds
\end{aligned}
\qquad (29)
$$

where we used the divergence theorem:

$$
\begin{aligned}
&\int_{\Omega}\boldsymbol{\sigma}^{T}\partial_{\mathbf{u}}(\delta\mathbf{u})\,d\Omega+\int_{\Omega}\delta\mathbf{u}^{T}\partial_{\mathbf{u}}^{T}\boldsymbol{\sigma}d\Omega=\int_{S_t}(\mathbf{n}_{\boldsymbol{\sigma}}\boldsymbol{\sigma})^{T}\delta\mathbf{u}ds\\
&\int_{\Omega}\mathbf{D}^{T}\partial_{\mathbf{e}}(\delta\varphi)\,d\Omega+\int_{\Omega}\delta\varphi\,\partial_{\mathbf{e}}^{T}\mathbf{D}d\Omega=\int_{S_Q}(\mathbf{n}_{\mathbf{e}}\mathbf{D})^{T}\delta\varphi ds\\
&\int_{\Omega}\mathbf{B}^{T}\partial_{\mathbf{m}}(\delta\psi)\,d\Omega+\int_{\Omega}\delta\psi\,\partial_{\mathbf{m}}^{T}\mathbf{B}d\Omega=\int_{S_B}(\mathbf{n}_{\mathbf{m}}\mathbf{B})^{T}\delta\psi ds
\end{aligned}
\qquad (30)
$$

to replace

$$\int_{\Omega} \boldsymbol{\sigma}^T \partial_{\mathbf{u}} (\delta \mathbf{u})\, d\Omega \text{ by } \int_{S_t} (\mathbf{n}_{\boldsymbol{\sigma}} \boldsymbol{\sigma})^T \delta \mathbf{u} ds - \int_{\Omega} \delta \mathbf{u}^T \partial_{\mathbf{u}}^T \boldsymbol{\sigma} d\Omega,$$

$$\int_{\Omega} \mathbf{D}^T \partial_{\mathbf{e}} (\delta \varphi)\, d\Omega \text{ by } \int_{S_Q} (\mathbf{n}_{\mathbf{e}} \mathbf{D})^T \delta \varphi ds - \int_{\Omega} \delta \varphi\, \partial_{\mathbf{e}}^T \mathbf{D} d\Omega$$

and

$$\int_{\Omega} \mathbf{B}^T \partial_{\mathbf{m}} (\delta \psi)\, d\Omega \text{ by } \int_{S_B} (\mathbf{n}_{\mathbf{m}} \mathbf{B})^T \delta \psi ds - \int_{\Omega} \delta \psi\, \partial_{\mathbf{m}}^T \mathbf{B} d\Omega.$$

Euler-Lagrange equations of this variational principle are the seven governing equations and six boundary conditions for magneto-electro-elasticity (eqs. (1) to (7) and eqs. (10) to (15)).

When the domain is composed of N sub-domains or finite elements ($\Omega = \sum_{i=1}^{N} \Omega^i$), the compatibility equations (eqs. (16), (18) and (20)) as well as the reciprocity equations (eqs. (17), (19) and (21)) should be satisfied on the sub-domain boundaries. Hence, the functional Π takes the form:

$$\Pi(\boldsymbol{\sigma}, \mathbf{D}, \mathbf{B}, \boldsymbol{\varepsilon}, \mathbf{E}, \mathbf{H}, \mathbf{u}, \varphi, \psi) = \sum_{i=1}^{N} \Pi_i(\boldsymbol{\sigma}^i, \mathbf{D}^i, \mathbf{B}^i, \boldsymbol{\varepsilon}^i, \mathbf{E}^i, \mathbf{H}^i, \mathbf{u}^i, \varphi^i, \psi^i)$$

$$\Pi = \sum_{i=1}^{N} \left(\begin{array}{l} \int\limits_{\Omega^i} \left[\frac{1}{2} \begin{Bmatrix} \boldsymbol{\varepsilon}^i \\ -\mathbf{E}^i \\ -\mathbf{H}^i \end{Bmatrix}^T \begin{bmatrix} \mathbf{C}^i & \mathbf{e}^{iT} & \mathbf{d}^{iT} \\ \mathbf{e}^i & -\mathbf{h}^i & -\mathbf{g}^{iT} \\ \mathbf{d}^i & -\mathbf{g}^i & -\boldsymbol{\mu}^i \end{bmatrix} \begin{Bmatrix} \boldsymbol{\varepsilon}^i \\ -\mathbf{E}^i \\ -\mathbf{H}^i \end{Bmatrix} \right. \\ \left. - \begin{Bmatrix} \boldsymbol{\sigma}^i \\ \mathbf{D}^i \\ \mathbf{B}^i \end{Bmatrix}^T \left(\begin{Bmatrix} \boldsymbol{\varepsilon}^i \\ -\mathbf{E}^i \\ -\mathbf{H}^i \end{Bmatrix} - \begin{Bmatrix} \partial_{\mathbf{u}} \mathbf{u}^i \\ \partial_{\mathbf{e}} \varphi^i \\ \partial_{\mathbf{m}} \psi^i \end{Bmatrix} \right) - \bar{\mathbf{b}}^T \mathbf{u}^i + \overline{\rho_f} \varphi^i \right] d\Omega \\ - \int\limits_{S_t^i} \bar{\mathbf{t}}^T \mathbf{u}^i ds - \int\limits_{S_Q^i} \bar{Q} \varphi^i ds - \int\limits_{S_u^i} (\mathbf{n}_{\boldsymbol{\sigma}}^i \boldsymbol{\sigma}^i)^T (\mathbf{u}^i - \bar{\mathbf{u}}) ds \\ - \int\limits_{S_\varphi^i} (\mathbf{n}_{\mathbf{e}}^i \mathbf{D}^i)^T (\varphi^i - \bar{\varphi}) ds - \int\limits_{S_\psi^i} (\mathbf{n}_{\mathbf{m}} \mathbf{B})^T (\psi - \bar{\psi}) ds \end{array} \right) \tag{31}$$

and its variation gives

$$\delta\Pi(\boldsymbol{\sigma}, \mathbf{D}, \mathbf{B}, \boldsymbol{\varepsilon}, \mathbf{E}, \mathbf{H}, \mathbf{u}, \varphi, \psi) = \sum_{i=1}^{N} \delta\Pi_i(\boldsymbol{\sigma}^i, \mathbf{D}^i, \mathbf{B}^i, \boldsymbol{\varepsilon}^i, \mathbf{E}^i, \mathbf{H}^i, \mathbf{u}^i, \varphi^i, \psi^i)$$

$$\delta\Pi = \sum_{i=1}^{N}$$
$$\left(\begin{array}{l}
\int\limits_{\Omega^i} \left[\left\{ \begin{array}{c} \delta\boldsymbol{\varepsilon}^i \\ -\delta\mathbf{E}^i \\ -\delta\mathbf{H}^i \end{array} \right\}^T \left(\left[\begin{array}{ccc} \mathbf{C}^i & \mathbf{e}^{iT} & \mathbf{d}^{iT} \\ \mathbf{e}^i & -\mathbf{h}^i & -\mathbf{g}^{iT} \\ \mathbf{d}^i & -\mathbf{g}^i & -\boldsymbol{\mu}^i \end{array} \right] \left\{ \begin{array}{c} \boldsymbol{\varepsilon}^i \\ -\mathbf{E}^i \\ -\mathbf{H}^i \end{array} \right\} - \left\{ \begin{array}{c} \boldsymbol{\sigma}^i \\ \mathbf{D}^i \\ \mathbf{B}^i \end{array} \right\}^T \right) \right. \\
\left. - \left\{ \begin{array}{c} \delta\boldsymbol{\sigma}^i \\ \delta\mathbf{D}^i \\ \delta\mathbf{B}^i \end{array} \right\}^T \left(\left\{ \begin{array}{c} \boldsymbol{\varepsilon}^i \\ -\mathbf{E}^i \\ -\mathbf{H}^i \end{array} \right\} - \left\{ \begin{array}{c} \partial_{\mathbf{u}}\mathbf{u}^i \\ \partial_{\mathbf{e}}\varphi^i \\ \partial_{\mathbf{m}}\psi^i \end{array} \right\} \right) - \left\{ \begin{array}{c} \delta\mathbf{u}^i \\ \delta\varphi^i \\ \delta\psi^i \end{array} \right\}^T \left\{ \begin{array}{c} \partial_{\mathbf{u}}^T\boldsymbol{\sigma}^i + \bar{\mathbf{b}} \\ \partial_{\mathbf{e}}^T\mathbf{D}^i - \overline{\rho_f} \\ \partial_{\mathbf{m}}^T\mathbf{B}^i \end{array} \right\} \right] d\Omega \\
- \int\limits_{S_t^i} (\mathbf{n}_{\boldsymbol{\sigma}}^i\boldsymbol{\sigma}^i - \bar{\mathbf{t}})^T\delta\mathbf{u}^i ds - \int\limits_{S_Q^i} (\mathbf{n}_{\mathbf{e}}^i\mathbf{D}^i - \bar{Q})\delta\varphi^i ds - \int\limits_{S_B^i} (\mathbf{n}_{\mathbf{m}}^i\mathbf{B}^i)\delta\psi ds \\
- \int\limits_{S_u^i} (\mathbf{n}_{\boldsymbol{\sigma}}^i\delta\boldsymbol{\sigma}^i)^T(\mathbf{u}^i - \bar{\mathbf{u}})ds - \int\limits_{S_\varphi^i} (\mathbf{n}_{\mathbf{e}}^i\delta\mathbf{D}^i)^T(\varphi^i - \bar{\varphi})ds - \int\limits_{S_\psi^i} (\mathbf{n}_{\mathbf{m}}^i\delta\mathbf{B}^i)^T(\psi^i - \bar{\psi})ds \\
- \int\limits_{S_m^i} \left[(\mathbf{n}_{\boldsymbol{\sigma}}^i\boldsymbol{\sigma}^i)^T\delta\mathbf{u}^i + (\mathbf{n}_{\mathbf{e}}^i\mathbf{D}^i)\delta\varphi^i + (\mathbf{n}_{\mathbf{m}}^i\mathbf{B}^i)\delta\psi^i \right] ds
\end{array} \right) \tag{32}$$

The three compatibility conditions (on displacement, electric potential and magnetic potential, eqs. (16), (18) and (20)), can be written now as:

$$\mathbf{u}^i = \mathbf{u}^j, \quad \varphi^i = \varphi^j \quad \text{and} \quad \psi^i = \psi^j \quad \text{at } S_m^{ij} \tag{33}$$

where S_m^{ij} is the boundary between subdomain i and subdomain j. Then,

$$\delta\mathbf{u}^i = \delta\mathbf{u}^j \ , \quad \delta\varphi^i = \delta\varphi^j \quad \text{and} \quad \delta\psi^i = \delta\psi^j \quad \text{at } S_m^{ij} \tag{34}$$

Hence, when we sum $\delta\Pi_i$ and $\delta\Pi_j$ in equation (32), the last term gives:

$$\int\limits_{S_m^{ij}} \left[(\mathbf{n}_{\boldsymbol{\sigma}}^i\boldsymbol{\sigma}^i + \mathbf{n}_{\boldsymbol{\sigma}}^j\boldsymbol{\sigma}^j)^T\delta\mathbf{u}^i + (\mathbf{n}_{\mathbf{e}}^i\mathbf{D}^i + \mathbf{n}_{\mathbf{e}}^j\mathbf{D}^j)\delta\varphi^i + (\mathbf{n}_{\mathbf{m}}^i\mathbf{B}^i + \mathbf{n}_{\mathbf{m}}^j\mathbf{B}^j)\delta\psi^i \right] ds$$

and the reciprocity conditions (eqs. (17), (19) and (21)) are also satisfied by the variational principle.

By selecting the mechanical displacements, electric potential and magnetic potential as the nodal variables in the finite element analysis, the essential boundary conditions (eqs. (11), (13) and (15)) can be easily enforced, and also the compatibility conditions (zeroth order continuity) of the displacements and electric and magnetic potentials (eq. (33)) are automatically satisfied *a priori*. Hence, the functional Π

can be simplified to:

$$\Pi = \sum \left(\int_{\Omega^i} \left[\frac{1}{2} \begin{Bmatrix} \boldsymbol{\varepsilon}^i \\ -\mathbf{E}^i \\ -\mathbf{H}^i \end{Bmatrix}^T \begin{bmatrix} \mathbf{C}^i & \mathbf{e}^{iT} & \mathbf{d}^{iT} \\ \mathbf{e}^i & -\mathbf{h}^i & -\mathbf{g}^{iT} \\ \mathbf{d}^i & -\mathbf{g}^i & -\boldsymbol{\mu}^i \end{bmatrix} \begin{Bmatrix} \boldsymbol{\varepsilon}^i \\ -\mathbf{E}^i \\ -\mathbf{H}^i \end{Bmatrix} \right.$$
$$- \begin{Bmatrix} \boldsymbol{\sigma}^i \\ \mathbf{D}^i \\ \mathbf{B}^i \end{Bmatrix}^T \left(\begin{Bmatrix} \boldsymbol{\varepsilon}^i \\ -\mathbf{E}^i \\ -\mathbf{H}^i \end{Bmatrix} - \begin{Bmatrix} \partial_{\mathbf{u}} \mathbf{u}^i \\ \partial_{\mathbf{e}} \varphi^i \\ \partial_{\mathbf{m}} \psi^i \end{Bmatrix} \right) - \bar{\mathbf{b}}^T \mathbf{u}^i + \overline{\rho_f} \varphi^i \Bigg] d\Omega$$
$$\left. - \int_{S_t^i} \bar{\mathbf{t}}^T \mathbf{u}^i ds - \int_{S_Q^i} \bar{Q} \varphi^i ds \right) \quad (35)$$

3.1 Primal finite elements

Expressing the strains using the strain-displacement eq. (4), the electric field intensity using the electric field- electric potential eq. (5) and the magnetic field intensity using the magnetic field- magnetic potential eq. (6), we get Π_1, a simplified version of the functional Π:

$$\Pi_1(\mathbf{u}^i, \varphi^i, \psi^i) = \sum_{i=1}^{N} \left(\begin{array}{l} \int_{\Omega^i} \left[\frac{1}{2} \begin{Bmatrix} \partial_{\mathbf{u}} \mathbf{u}^i \\ \partial_{\mathbf{e}} \varphi^i \\ \partial_{\mathbf{m}} \psi^i \end{Bmatrix}^T \begin{bmatrix} \mathbf{C}^i & \mathbf{e}^{iT} & \mathbf{d}^{iT} \\ \mathbf{e}^i & -\mathbf{h}^i & -\mathbf{g}^{iT} \\ \mathbf{d}^i & -\mathbf{g}^i & -\boldsymbol{\mu}^i \end{bmatrix} \begin{Bmatrix} \partial_{\mathbf{u}} \mathbf{u}^i \\ \partial_{\mathbf{e}} \varphi^i \\ \partial_{\mathbf{m}} \psi^i \end{Bmatrix} \right. \\ \left. - \bar{\mathbf{b}}^T \mathbf{u}^i + \overline{\rho_f} \varphi^i \right] d\Omega - \int_{S_t^i} \bar{\mathbf{t}}^T \mathbf{u}^i ds - \int_{S_Q^i} \bar{Q} \varphi^i ds \end{array} \right) \quad (36)$$

This functional requires only the displacements $\mathbf{u}^i$, electric potential φ^i, and magnetic potential ψ^i to be assumed in each element, and is known as the primal or irreducible formulation for magneto-electro-elasticity (irreducible in the sense that the number of field variables cannot be further reduced). The superscript i will be dropped from now on, for simplicity, i.e., $\mathbf{u}$,φ, ψ will be used instead of $\mathbf{u}^i$,φ^i, ψ^i to express the primal variables in each element.

In the primal finite element analysis, the mechanical displacements, electric and magnetic potentials in each element are assumed in terms of the nodal values of the displacements, electric and magnetic potentials respectively through the use of the isoparametric shape (interpolation) functions as:

$$\mathbf{u} = \mathbf{N}_{\mathbf{u}}(\xi^\gamma)\mathbf{q}_{\mathbf{u}} \quad \varphi = \mathbf{N}_{\boldsymbol{\varphi}}(\xi^\gamma)\mathbf{q}_{\boldsymbol{\varphi}} \quad \psi = \mathbf{N}_{\boldsymbol{\psi}}(\xi^\gamma)\mathbf{q}_{\boldsymbol{\psi}} \quad (37)$$

where ξ^γ, $\gamma = 1,2$ are the element-fixed local non-dimensional curvilinear coordinates, $\mathbf{N}_{\mathbf{u}}(\xi^\gamma)$, $\mathbf{N}_{\boldsymbol{\varphi}}(\xi^\gamma)$ and $\mathbf{N}_{\boldsymbol{\psi}}(\xi^\gamma)$ are the displacement, electric and magnetic

potentials shape functions respectively, and $\mathbf{q_u}$, $\mathbf{q_\varphi}$ and $\mathbf{q_\psi}$ are the vectors of element nodal displacements, electric and magnetic potentials respectively.

The strain-field, intensity of electric and magnetic fields derived from the primal variables are then expressed as:

$$\begin{aligned}
&\boldsymbol{\varepsilon}^P = \boldsymbol{\partial}_\mathbf{u}\mathbf{u} = \boldsymbol{\partial}_\mathbf{u}(\mathbf{N_u}(\xi^\gamma)\mathbf{q_u}) = \mathbf{B_u}(\xi^\gamma)\mathbf{q_u} \\
&-\mathbf{E}^P = \boldsymbol{\partial}_\mathbf{e}\varphi = \boldsymbol{\partial}_\mathbf{e}(\mathbf{N_\varphi}(\xi^\gamma)\mathbf{q_\varphi}) = \mathbf{B_\varphi}(\xi^\gamma)\mathbf{q_\varphi} \\
&-\mathbf{H}^P = \boldsymbol{\partial}_\mathbf{m}\psi = \boldsymbol{\partial}_\mathbf{m}(\mathbf{N_\psi}(\xi^\gamma)\mathbf{q_\psi}) = \mathbf{B_\psi}(\xi^\gamma)\mathbf{q_\psi}
\end{aligned} \tag{38}$$

where $\mathbf{B_u}(\xi^\gamma) = \boldsymbol{\partial}_\mathbf{u}\mathbf{N_u}(\xi^\gamma), \mathbf{B_\varphi}(\xi^\gamma) = \boldsymbol{\partial}_\mathbf{e}\mathbf{N_\varphi}(\xi^\gamma)$ and $\mathbf{B_\psi}(\xi^\gamma) = \boldsymbol{\partial}_\mathbf{m}\mathbf{N_\psi}(\xi^\gamma)$.

Substituting this into the functional Π_1, and dropping $(\xi^\gamma)$for simplicity, we get:

$$\begin{aligned}
\Pi_1 = \sum \Bigg(& \frac{1}{2}\begin{Bmatrix}\mathbf{q_u}\\ \mathbf{q_\varphi}\\ \mathbf{q_\psi}\end{Bmatrix}^T \begin{bmatrix} \int_\Omega \mathbf{B_u}^T\mathbf{C}\mathbf{B_u}d\Omega & \int_\Omega \mathbf{B_u}^T\mathbf{e}^T\mathbf{B_\varphi}d\Omega & \int_\Omega \mathbf{B_u}^T\mathbf{d}^T\mathbf{B_\psi}d\Omega \\ \int_\Omega \mathbf{B_\varphi}^T\mathbf{e}\mathbf{B_u}d\Omega & -\int_\Omega \mathbf{B_\varphi}^T\mathbf{h}\mathbf{B_\varphi}d\Omega & -\int_\Omega \mathbf{B_\varphi}^T\mathbf{g}^T\mathbf{B_\psi}d\Omega \\ \int_\Omega \mathbf{B_\psi}^T\mathbf{d}\mathbf{B_u}d\Omega & -\int_\Omega \mathbf{B_\psi}^T\mathbf{g}\mathbf{B_\varphi}d\Omega & -\int_\Omega \mathbf{B_\psi}^T\mu\mathbf{B_\psi}d\Omega \end{bmatrix} \begin{Bmatrix}\mathbf{q_u}\\ \mathbf{q_\varphi}\\ \mathbf{q_\psi}\end{Bmatrix} \\
& - \left(\int_\Omega \bar{\mathbf{b}}^T\mathbf{N_u}d\Omega\right)\mathbf{q_u} + \left(\int_\Omega \overline{\rho_f}\mathbf{N_\varphi}d\Omega\right)\mathbf{q_\varphi} - \left(\int_{S_t} \bar{\mathbf{t}}^T\mathbf{N_u}ds\right)\mathbf{q_u} - \left(\int_{S_Q} \bar{Q}\mathbf{N_\varphi}ds\right)\mathbf{q_\varphi} \Bigg)
\end{aligned} \tag{39}$$

Equating its variation to zero gives the finite element equation:

$$\mathbf{K}\mathbf{q} = \mathbf{F} \tag{40}$$

where $\mathbf{q} = \begin{Bmatrix}\mathbf{q_u} & \mathbf{q_\varphi} & \mathbf{q_\psi}\end{Bmatrix}^T$ and

$$\begin{aligned}
\mathbf{K} &= \begin{bmatrix} \mathbf{K_{uu}} & \mathbf{K_{u\varphi}} & \mathbf{K_{u\psi}} \\ \mathbf{K_{u\varphi}^T} & -\mathbf{K_{\varphi\varphi}} & -\mathbf{K_{\varphi\psi}} \\ \mathbf{K_{u\psi}^T} & -\mathbf{K_{\varphi\psi}^T} & -\mathbf{K_{\psi\psi}} \end{bmatrix} \\
&= \begin{bmatrix} \int_\Omega \mathbf{B_u}^T\mathbf{C}\mathbf{B_u}d\Omega & \int_\Omega \mathbf{B_u}^T\mathbf{e}^T\mathbf{B_\varphi}d\Omega & \int_\Omega \mathbf{B_u}^T\mathbf{d}^T\mathbf{B_\psi}d\Omega \\ \int_\Omega \mathbf{B_\varphi}^T\mathbf{e}\mathbf{B_u}d\Omega & -\int_\Omega \mathbf{B_\varphi}^T\mathbf{h}\mathbf{B_\varphi}d\Omega & -\int_\Omega \mathbf{B_\varphi}^T\mathbf{g}^T\mathbf{B_\psi}d\Omega \\ \int_\Omega \mathbf{B_\psi}^T\mathbf{d}\mathbf{B_u}d\Omega & -\int_\Omega \mathbf{B_\psi}^T\mathbf{g}\mathbf{B_\varphi}d\Omega & -\int_\Omega \mathbf{B_\psi}^T\boldsymbol{\mu}\mathbf{B_\psi}d\Omega \end{bmatrix}
\end{aligned} \tag{41}$$

$$\mathbf{F} = \begin{Bmatrix}\mathbf{F_u}\\ \mathbf{F_\varphi}\\ \mathbf{0}\end{Bmatrix} = \begin{Bmatrix} \int_\Omega \bar{\mathbf{b}}^T\mathbf{N_u}d\Omega + \int_{S_t} \bar{\mathbf{t}}^T\mathbf{N_u}ds \\ -\int_\Omega \overline{\rho_f}\mathbf{N_\varphi}d\Omega + \int_{S_Q} \bar{Q}\mathbf{N_\varphi}ds \\ \mathbf{0} \end{Bmatrix} \tag{42}$$

We call this element "Primal finite element" ("PFEM") for magneto-electro-elastic (MEE) materials. Finite elements based on the irreducible formulation for magneto-electro-elasticity are similar to the displacement based finite elements for elasticity. They suffer from having high stiffness, very sensitive to mesh distortion and aspect ratio and that the shear and normal strains are "locked" together. The various hybrid/mixed elements for piezoelectricity in the literature use multi-field variational principles.

3.2 Hybrid/mixed finite elements for magneto-electro-elastic materials using independently assumed strain, electric and magnetic fields

3.2.1 Local orthogonal base vectors

In order to assume an independent strain field (which is a second order tensor) as well as electric and magnetic field intensities (which are vectors), we have to define the components of these fields as well as their base vectors. The components of these fields will be assumed in the element-fixed local non-dimensional curvilinear coordinates $\xi^1 - \xi^3$, as shown in Figure 1 for the simple case of four-node quadrilateral element. As for the base vectors, we cannot use the covariant base vectors $\mathbf{g_1} - \mathbf{g_3}$ in the directions of the local non-dimensional curvilinear coordinates $\xi^1 - \xi^3$ since they are not orthogonal. It is required to define an element-fixed local orthogonal base vectors so that the element properties, such as the eigenvalues of the stiffness matrix, are not changed according to the orientation of the global Cartesian coordinate system, or the observer's point of view. Whatever the rotation of the global Cartesian coordinate system $x_1 - x_2 - x_3$, the element-fixed local curvilinear coordinates $\xi^1 - \xi^3$, as well as the element-fixed local orthogonal base vectors, denoted $\hat{\mathbf{g}}_\mathbf{1} - \hat{\mathbf{g}}_\mathbf{3}$, are kept invariant. These element-fixed local orthogonal base vectors, $\hat{\mathbf{g}}_\mathbf{1} - \hat{\mathbf{g}}_\mathbf{3}$, are defined as follows: $\hat{\mathbf{g}}_\mathbf{1}$ is in the same direction of the covariant base vector $\mathbf{g_1}$ evaluated at the center (0, 0), and $\hat{\mathbf{g}}_\mathbf{3}$ is obtained by rotating $\hat{\mathbf{g}}_\mathbf{1}$ around $-\mathbf{e_2}$ counterclockwise by 90^o.

Using the isoparametric representation:

$$x_i = \sum_n x_i^{(n)} N^{(n)}(\xi^\gamma) \tag{43}$$

where x_i are the global Cartesian coordinates, $x_i^{(n)}$ are the Cartesian coordinates of the element nodes, and from the position vector $\mathbf{R} = x_1\mathbf{e_1} + x_3\mathbf{e_3}$, $\mathbf{g_1}$ can be obtained through the relation:

$$\mathbf{g_1} = \frac{\partial \mathbf{R}}{\partial \xi^1} = \frac{\partial x_1}{\partial \xi^1}\mathbf{e_1} + \frac{\partial x_3}{\partial \xi^1}\mathbf{e_3} = \sum_n \left(\frac{\partial N^{(n)}(\xi^1, \xi^3)}{\partial \xi^1} x_1^{(n)} \mathbf{e_1} + \frac{\partial N^{(n)}(\xi^1, \xi^3)}{\partial \xi^1} x_2^{(n)} \mathbf{e_3} \right)$$

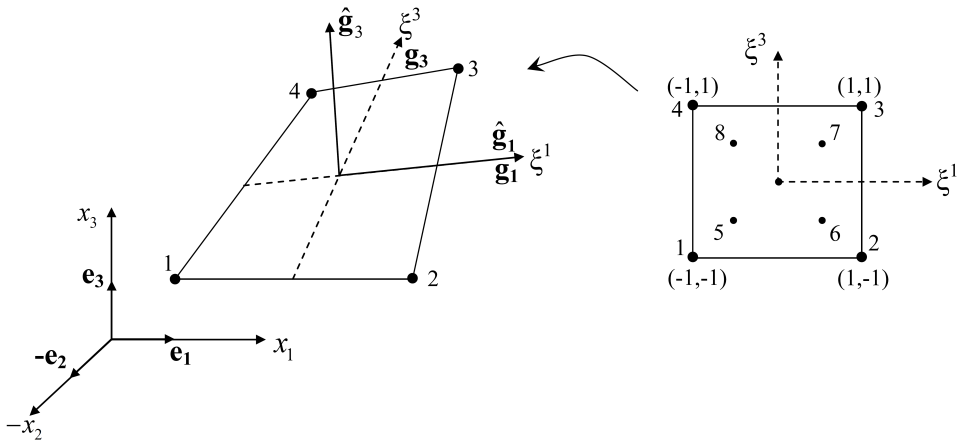

Figure 1: Global Cartesian coordinates $x_1 - x_2 - x_3$, curvilinear coordinates $\xi^1 - \xi^3$, and element-fixed local orthogonal base vectors $\hat{\mathbf{g}}_1 - \hat{\mathbf{g}}_3$ for the four-node quadrilateral finite element

(44)

Then, $\hat{\mathbf{g}}_\mathbf{1}$ and $\hat{\mathbf{g}}_\mathbf{3}$ can be written as:

$$\hat{\mathbf{g}}_\mathbf{1} = \mathbf{g_1}(0,0) = \sum_n \left(\frac{\partial N^{(n)}}{\partial \xi^1}(0,0) x_1^{(n)} \mathbf{e_1} + \frac{\partial N^{(n)}}{\partial \xi^1}(0,0) x_3^{(n)} \mathbf{e_3} \right) \tag{45}$$

$$\hat{\mathbf{g}}_\mathbf{3} = -\mathbf{e_2} \times \hat{\mathbf{g}}_1 = \sum_n \left(-\frac{\partial N^{(n)}}{\partial \xi^1}(0,0) x_3^{(n)} \mathbf{e_1} + \frac{\partial N^{(n)}}{\partial \xi^1}(0,0) x_1^{(n)} \mathbf{e_3} \right) \tag{46}$$

Figure 1 shows the four-node quadrilateral element in global Cartesian coordinates $x_1 - x_2 - x_3$ in the direction of the orthogonal base vectors $\mathbf{e_1} - \mathbf{e_2} - \mathbf{e_3}$, the element-fixed local curvilinear coordinates $\xi^1 - \xi^3$ and the covariant base vectors $\mathbf{g_1} - \mathbf{g_3}$ in their directions, and the element-fixed local orthogonal base vectors $\hat{\mathbf{g}}_\mathbf{1} - \hat{\mathbf{g}}_\mathbf{3}$. The isoparametric mapping transforms the regular element in the non-dimensional coordinates $\xi^1 - \xi^3$ that varies from -1 to 1 into the irregular element in the Cartesian $x_1 - x_3$ coordinates.

With the base vectors being defined, the strain tensor and the electric and magnetic fields vectors can be expressed in any coordinate system and its associated base vectors:

$$\boldsymbol{\varepsilon} = \varepsilon_{ij} \mathbf{e_i} \mathbf{e_j} = \hat{\varepsilon}^{kl} \hat{\mathbf{g}}_\mathbf{k} \hat{\mathbf{g}}_\mathbf{l}, \quad \mathbf{E} = E_i \mathbf{e_i} = \hat{E}^k \hat{\mathbf{g}}_\mathbf{k}, \quad \mathbf{H} = H_i \mathbf{e_i} = \hat{H}^k \hat{\mathbf{g}}_\mathbf{k} \tag{47}$$

The transformation of the strain components from the element-fixed local orthogonal coordinates to the global Cartesian coordinates follows this relation;

$$\varepsilon_{ij} = \hat{\varepsilon}^{kl}(\hat{\mathbf{g}}_\mathbf{k}.\mathbf{e}_\mathbf{i})(\hat{\mathbf{g}}_\mathbf{l}.\mathbf{e}_\mathbf{j}) \tag{48}$$

Using the fact that $\varepsilon_{ij} = \varepsilon_{ji}$ and $\hat{\varepsilon}^{kl} = \hat{\varepsilon}^{lk}$, eq. (48) can be written as:

$$\begin{Bmatrix} \varepsilon_1 \\ \varepsilon_3 \\ 2\varepsilon_5 \end{Bmatrix} = \begin{bmatrix} (\hat{\mathbf{g}}_1.\mathbf{e}_1)^2 & (\hat{\mathbf{g}}_3.\mathbf{e}_1)^2 & (\hat{\mathbf{g}}_1.\mathbf{e}_1)(\hat{\mathbf{g}}_3.\mathbf{e}_1) \\ (\hat{\mathbf{g}}_1.\mathbf{e}_3)^2 & (\hat{\mathbf{g}}_3.\mathbf{e}_3)^2 & (\hat{\mathbf{g}}_1.\mathbf{e}_3)(\hat{\mathbf{g}}_3.\mathbf{e}_3) \\ 2(\hat{\mathbf{g}}_1.\mathbf{e}_1)(\hat{\mathbf{g}}_1.\mathbf{e}_3) & 2(\hat{\mathbf{g}}_3.\mathbf{e}_1)(\hat{\mathbf{g}}_3.\mathbf{e}_3) & (\hat{\mathbf{g}}_1.\mathbf{e}_1)(\hat{\mathbf{g}}_3.\mathbf{e}_3) + (\hat{\mathbf{g}}_3.\mathbf{e}_1)(\hat{\mathbf{g}}_1.\mathbf{e}_3) \end{bmatrix} \begin{Bmatrix} \hat{\varepsilon}^1 \\ \hat{\varepsilon}^3 \\ 2\hat{\varepsilon}^5 \end{Bmatrix} \tag{49}$$

or, $\boldsymbol{\varepsilon} = \mathbf{T}_{\boldsymbol{\varepsilon}}\hat{\boldsymbol{\varepsilon}}$.

Note that in ε_{ij}, $ij = 11, 33, 13$ corresponds to ε_k, $k = 1, 3, 5$.

Similarly, the transformation of the components of the electric and magnetic fields from the element-fixed local orthogonal coordinates to the global Cartesian coordinates follows:

$$\begin{Bmatrix} E_1 \\ E_3 \end{Bmatrix} = \begin{bmatrix} (\hat{\mathbf{g}}_1.\mathbf{e}_1)^2 & (\hat{\mathbf{g}}_3.\mathbf{e}_1)^2 \\ (\hat{\mathbf{g}}_1.\mathbf{e}_3)^2 & (\hat{\mathbf{g}}_3.\mathbf{e}_3)^2 \end{bmatrix} \begin{Bmatrix} \hat{E}^1 \\ \hat{E}^3 \end{Bmatrix} \tag{50}$$

or, $\mathbf{E} = \mathbf{T}_\mathbf{E}\hat{\mathbf{E}}$

$$\begin{Bmatrix} H_1 \\ H_3 \end{Bmatrix} = \begin{bmatrix} (\hat{\mathbf{g}}_1.\mathbf{e}_1)^2 & (\hat{\mathbf{g}}_3.\mathbf{e}_1)^2 \\ (\hat{\mathbf{g}}_1.\mathbf{e}_3)^2 & (\hat{\mathbf{g}}_3.\mathbf{e}_3)^2 \end{bmatrix} \begin{Bmatrix} \hat{H}^1 \\ \hat{H}^3 \end{Bmatrix} \tag{51}$$

or, $\mathbf{H} = \mathbf{T}_\mathbf{H}\hat{\mathbf{H}}$

where $\mathbf{T}_{\boldsymbol{\varepsilon}}$, $\mathbf{T}_\mathbf{E}$ and $\mathbf{T}_\mathbf{H}$ are the transformation matrices that relate the components of strain, electric and magnetic fields, respectively, in the Cartesian coordinate system to that of the local orthogonal coordinate system. Note that these transformation matrices reduce to the identity matrix for rectangular shaped elements because in this case, $\hat{\mathbf{g}}_1$ is in the direction of $\mathbf{e}_1$ and $\hat{\mathbf{g}}_3$ is in the direction of $\mathbf{e}_3$. So if the elements are of a rectangular shape, there is no need to use the transformation matrices.

3.2.2 Independently assumed strain, electric and magnetic fields

Now since we defined covariant base vectors, the contravariant components of the independently assumed strain, electric and magnetic fields in the local non-dimensional curvilinear coordinates $\xi^1 - \xi^3$ can be written as:

$$\hat{\boldsymbol{\varepsilon}}^{In} = \mathbf{A}_{\boldsymbol{\varepsilon}}(\xi^\gamma)\boldsymbol{\alpha} \qquad -\hat{\mathbf{E}}^{In} = \mathbf{A}_\mathbf{E}(\xi^\gamma)\boldsymbol{\beta} \qquad -\hat{\mathbf{H}}^{In} = \mathbf{A}_\mathbf{H}(\xi^\gamma)\boldsymbol{\gamma} \tag{52}$$

where $\boldsymbol{\alpha}$, $\boldsymbol{\beta}$ and $\boldsymbol{\gamma}$ are undetermined parameters.

For 2D four-node quadrilateral element, the normal strain in the 1-direction is assumed as:

$$\hat{\varepsilon}^{In1} = \alpha_1 + \alpha_2\xi^1 + \alpha_3\xi^3 + \alpha_4\xi^1\xi^3 = \mathbf{A}_{\boldsymbol{\varepsilon 1}}(\xi^\gamma)\boldsymbol{\alpha}_{\mathbf{I}} \tag{53}$$

where $\mathbf{A}_{\boldsymbol{\varepsilon 1}}(\xi^\gamma) = \begin{bmatrix} 1 & \xi^1 & \xi^3 & \xi^1\xi^3 \end{bmatrix}$ and $\boldsymbol{\alpha}_{\mathbf{I}} = \begin{bmatrix} \alpha_1 & \alpha_2 & \alpha_3 & \alpha_4 \end{bmatrix}^T$.

Similarly the normal strain in the 3- direction and the shear strain:

$$\hat{\varepsilon}^{In3} = \mathbf{A}_{\boldsymbol{\varepsilon 3}}(\xi^\gamma)\boldsymbol{\alpha}_{\mathbf{II}}, \quad \varepsilon^{In5} = \mathbf{A}_{\boldsymbol{\varepsilon 5}}(\xi^\gamma)\boldsymbol{\alpha}_{\mathbf{III}} \tag{54}$$

where $\mathbf{A}_{\varepsilon 3}(\xi^\gamma) = \begin{bmatrix} 1 & \xi^1 & \xi^3 & \xi^1\xi^3 \end{bmatrix}$, $\mathbf{A}_{\varepsilon 5}(\xi^\gamma) = 1$, $\boldsymbol{\alpha}_{\mathbf{II}} = \begin{bmatrix} \alpha_5 & \alpha_6 & \alpha_7 & \alpha_8 \end{bmatrix}^T$, and $\boldsymbol{\alpha}_{\mathbf{III}} = \alpha_9$.

The independent electric field can also be assumed as:

$$-\hat{E}^{In1} = \mathbf{A}_{\mathbf{E1}}(\xi^\gamma)\boldsymbol{\beta}_{\mathbf{I}}, \qquad -\hat{E}^{In3} = \mathbf{A}_{\mathbf{E3}}(\xi^\gamma)\boldsymbol{\beta}_{\mathbf{II}} \tag{55}$$

where $\mathbf{A}_{\mathbf{E1}}(\xi^\gamma) = \mathbf{A}_{\mathbf{E3}}(\xi^\gamma) = \begin{bmatrix} 1 & \xi^1 & \xi^3 & \xi^1\xi^3 \end{bmatrix}$, $\boldsymbol{\beta}_{\mathbf{I}} = \begin{bmatrix} \beta_1 & \beta_2 & \beta_3 & \beta_4 \end{bmatrix}^T$ and $\boldsymbol{\beta}_{\mathbf{II}} = \begin{bmatrix} \beta_5 & \beta_6 & \beta_7 & \beta_8 \end{bmatrix}^T$.

and the independent magnetic field as:

$$-\hat{H}^{In1} = \mathbf{A}_{\mathbf{H1}}(\xi^\gamma)\boldsymbol{\gamma}_{\mathbf{I}} \quad -\hat{H}^{In2} = \mathbf{A}_{\mathbf{H2}}(\xi^\gamma)\boldsymbol{\gamma}_{\mathbf{II}} \tag{56}$$

where $\mathbf{A}_{\mathbf{H1}}(\xi^\gamma) = \mathbf{A}_{\mathbf{H2}}(\xi^\gamma) = \begin{bmatrix} 1 & \xi^1 & \xi^3 & \xi^1\xi^3 \end{bmatrix}$, $\boldsymbol{\gamma}_{\mathbf{I}} = \begin{bmatrix} \gamma_1 & \gamma_2 & \gamma_3 & \gamma_4 \end{bmatrix}^T$ and $\boldsymbol{\gamma}_{\mathbf{II}} = \begin{bmatrix} \gamma_5 & \gamma_6 & \gamma_7 & \gamma_8 \end{bmatrix}^T$.

3.2.3 HMFEM using Atluri's variational principle

The stress, electric displacement and magnetic induction fields can be eliminated from the functional Π in eq. (35) using the constitutive law to get:

$$\begin{aligned}
&\Pi_2(\boldsymbol{\varepsilon}, \mathbf{E}, \mathbf{H}, \mathbf{u}, \varphi, \psi) = \\
&\int_\Omega \left[\frac{1}{2} \begin{Bmatrix} \boldsymbol{\varepsilon} \\ -\mathbf{E} \\ -\mathbf{H} \end{Bmatrix}^T \begin{bmatrix} \mathbf{C} & \mathbf{e}^T & \mathbf{d}^T \\ \mathbf{e} & -\mathbf{h} & -\mathbf{g}^T \\ \mathbf{d} & -\mathbf{g} & -\boldsymbol{\mu} \end{bmatrix} \begin{Bmatrix} \boldsymbol{\varepsilon} \\ -\mathbf{E} \\ -\mathbf{H} \end{Bmatrix} \right. \\
&- \begin{Bmatrix} \boldsymbol{\varepsilon} \\ -\mathbf{E} \\ -\mathbf{H} \end{Bmatrix}^T \begin{bmatrix} \mathbf{C} & \mathbf{e}^T & \mathbf{d}^T \\ \mathbf{e} & -\mathbf{h} & -\mathbf{g}^T \\ \mathbf{d} & -\mathbf{g} & -\boldsymbol{\mu} \end{bmatrix}^T \left(\begin{Bmatrix} \boldsymbol{\varepsilon} \\ -\mathbf{E} \\ -\mathbf{H} \end{Bmatrix} - \begin{Bmatrix} \partial_{\mathbf{u}}\mathbf{u} \\ \partial_{\mathbf{e}}\varphi \\ \partial_{\mathbf{m}}\psi \end{Bmatrix} \right) \\
&\left. - \bar{\mathbf{b}}^T\mathbf{u} + \overline{\rho_f}\varphi \right] d\Omega - \int_{S_t} \bar{\mathbf{t}}^T\mathbf{u} ds - \int_{S_Q} \bar{Q}\varphi ds
\end{aligned} \tag{57}$$

This can be seen as the extension of "Atluri's variational principle" [see Atluri (1975)] and can be written as:

$$\Pi_2(\boldsymbol{\varepsilon},\mathbf{E},\mathbf{H},\mathbf{u},\varphi,\psi) = \int_\Omega \left[-\frac{1}{2} \begin{Bmatrix} \boldsymbol{\varepsilon} \\ -\mathbf{E} \\ -\mathbf{H} \end{Bmatrix}^T \begin{bmatrix} \mathbf{C} & \mathbf{e}^T & \mathbf{d}^T \\ \mathbf{e} & -\mathbf{h} & -\mathbf{g}^T \\ \mathbf{d} & -\mathbf{g} & -\boldsymbol{\mu} \end{bmatrix} \begin{Bmatrix} \boldsymbol{\varepsilon} \\ -\mathbf{E} \\ -\mathbf{H} \end{Bmatrix} + \begin{Bmatrix} \partial_{\mathbf{u}}\mathbf{u} \\ \partial_{\mathbf{e}}\varphi \\ \partial_{\mathbf{m}}\psi \end{Bmatrix}^T \begin{bmatrix} \mathbf{C} & \mathbf{e}^T & \mathbf{d}^T \\ \mathbf{e} & -\mathbf{h} & -\mathbf{g}^T \\ \mathbf{d} & -\mathbf{g} & -\boldsymbol{\mu} \end{bmatrix} \begin{Bmatrix} \boldsymbol{\varepsilon} \\ -\mathbf{E} \\ -\mathbf{H} \end{Bmatrix} - \bar{\mathbf{b}}^T\mathbf{u} + \overline{\rho_f}\varphi \Big] d\Omega - \int_{S_t} \bar{\mathbf{t}}^T\mathbf{u}\, ds - \int_{S_Q} \bar{Q}\varphi\, ds \quad (58)$$

Beside using the mechanical displacement, the electric and magnetic potential representation as in eq. (37), we also use the independently assumed strain, electric and magnetic fields in eqs. (52). If the element shape is not rectangular, these independently assumed fields should be transformed to the Cartesian coordinate system first (using the transformation matrices defined in subsection 3.2.1) in order to be used in the variational principle:

$$\begin{aligned} \boldsymbol{\varepsilon}^{In} &= \mathbf{T}_{\boldsymbol{\varepsilon}}\hat{\boldsymbol{\varepsilon}}^{In} = \mathbf{T}_{\boldsymbol{\varepsilon}}\mathbf{A}_{\boldsymbol{\varepsilon}}(\xi^\gamma)\boldsymbol{\alpha} \\ -\mathbf{H}^{In} &= -\mathbf{T}_{\mathbf{H}}\hat{\mathbf{H}}^{In} = \mathbf{T}_{\mathbf{H}}\mathbf{A}_{\mathbf{H}}(\xi^\gamma)\boldsymbol{\gamma} \\ -\mathbf{E}^{In} &= -\mathbf{T}_{\mathbf{E}}\hat{\mathbf{E}}^{In} = \mathbf{T}_{\mathbf{E}}\mathbf{A}_{\mathbf{E}}(\xi^\gamma)\boldsymbol{\beta} \end{aligned} \quad (59)$$

The functional Π_2 in eq. (58) becomes:

$$\Pi_2(\boldsymbol{\varepsilon},\mathbf{E},\mathbf{H},\mathbf{u},\varphi,\psi) = -\frac{1}{2} \begin{Bmatrix} \boldsymbol{\alpha} \\ \boldsymbol{\beta} \\ \boldsymbol{\gamma} \end{Bmatrix}^T \mathbf{H} \begin{Bmatrix} \boldsymbol{\alpha} \\ \boldsymbol{\beta} \\ \boldsymbol{\gamma} \end{Bmatrix} + \begin{Bmatrix} \mathbf{q}_{\mathbf{u}} \\ \mathbf{q}_{\boldsymbol{\varphi}} \\ \mathbf{q}_{\boldsymbol{\psi}} \end{Bmatrix}^T \mathbf{G}^T \begin{Bmatrix} \boldsymbol{\alpha} \\ \boldsymbol{\beta} \\ \boldsymbol{\gamma} \end{Bmatrix} - \begin{Bmatrix} \mathbf{q}_{\mathbf{u}} \\ \mathbf{q}_{\boldsymbol{\varphi}} \\ \mathbf{q}_{\boldsymbol{\psi}} \end{Bmatrix}^T \mathbf{F} \quad (60)$$

where

$$\mathbf{H} = \int_\Omega \begin{bmatrix} \mathbf{A}_{\boldsymbol{\varepsilon}}^T(\xi^\gamma)\mathbf{C}\mathbf{A}_{\boldsymbol{\varepsilon}}(\xi^\gamma) & \mathbf{A}_{\boldsymbol{\varepsilon}}^T(\xi^\gamma)\mathbf{e}^T\mathbf{A}_{\mathbf{E}}(\xi^\gamma) & \mathbf{A}_{\boldsymbol{\varepsilon}}^T(\xi^\gamma)\mathbf{d}^T\mathbf{A}_{\mathbf{H}}(\xi^\gamma) \\ \mathbf{A}_{\mathbf{E}}^T(\xi^\gamma)\mathbf{e}\mathbf{A}_{\boldsymbol{\varepsilon}}(\xi^\gamma) & -\mathbf{A}_{\mathbf{E}}^T(\xi^\gamma)\mathbf{h}\mathbf{A}_{\mathbf{E}}(\xi^\gamma) & -\mathbf{A}_{\mathbf{E}}^T(\xi^\gamma)\mathbf{g}^T\mathbf{A}_{\mathbf{H}}(\xi^\gamma) \\ \mathbf{A}_{\mathbf{H}}^T(\xi^\gamma)\mathbf{d}\mathbf{A}_{\boldsymbol{\varepsilon}}(\xi^\gamma) & -\mathbf{A}_{\mathbf{H}}^T(\xi^\gamma)\mathbf{g}\mathbf{A}_{\mathbf{E}}(\xi^\gamma) & -\mathbf{A}_{\mathbf{H}}^T(\xi^\gamma)\mu\mathbf{A}_{\mathbf{H}}(\xi^\gamma) \end{bmatrix} d\Omega \quad (61)$$

$$\mathbf{G} = \int_\Omega \begin{bmatrix} \mathbf{A}_{\boldsymbol{\varepsilon}}^T(\xi^\gamma)\mathbf{T}_{\boldsymbol{\varepsilon}}^T\mathbf{C}\mathbf{B}_{\mathbf{u}}(\xi^\gamma) & \mathbf{A}_{\boldsymbol{\varepsilon}}^T(\xi^\gamma)\mathbf{T}_{\boldsymbol{\varepsilon}}^T\mathbf{e}^T\mathbf{B}_{\boldsymbol{\varphi}}(\xi^\gamma) & \mathbf{A}_{\boldsymbol{\varepsilon}}^T(\xi^\gamma)\mathbf{T}_{\boldsymbol{\varepsilon}}^T\mathbf{d}^T\mathbf{B}_{\boldsymbol{\psi}}(\xi^\gamma) \\ \mathbf{A}_{\mathbf{E}}^T(\xi^\gamma)\mathbf{T}_{\mathbf{E}}^T\mathbf{e}\mathbf{B}_{\mathbf{u}}(\xi^\gamma) & -\mathbf{A}_{\mathbf{E}}^T(\xi^\gamma)\mathbf{T}_{\mathbf{E}}^T\mathbf{h}^T\mathbf{B}_{\boldsymbol{\varphi}}(\xi^\gamma) & -\mathbf{A}_{\mathbf{E}}^T(\xi^\gamma)\mathbf{T}_{\mathbf{E}}^T\mathbf{g}^T\mathbf{B}_{\boldsymbol{\psi}}(\xi^\gamma) \\ \mathbf{A}_{\mathbf{H}}^T(\xi^\gamma)\mathbf{T}_{\mathbf{H}}^T\mathbf{d}\mathbf{B}_{\mathbf{u}}(\xi^\gamma) & -\mathbf{A}_{\mathbf{H}}^T(\xi^\gamma)\mathbf{T}_{\mathbf{H}}^T\mathbf{g}\mathbf{B}_{\boldsymbol{\varphi}}(\xi^\gamma) & -\mathbf{A}_{\mathbf{H}}^T(\xi^\gamma)\mathbf{T}_{\mathbf{H}}^T\mu\mathbf{B}_{\boldsymbol{\psi}}(\xi^\gamma) \end{bmatrix} d\Omega \quad (62)$$

and $\mathbf{F}$ is defined in eq. (42).

In eq. (61) we used the identities:

$$\mathbf{T}_{\boldsymbol{\varepsilon}}^{T}\mathbf{C}\mathbf{T}_{\boldsymbol{\varepsilon}}=\mathbf{C},\quad \mathbf{T}_{\mathbf{E}}^{T}\mathbf{e}\mathbf{T}_{\boldsymbol{\varepsilon}}=\mathbf{e},\quad \mathbf{T}_{\mathbf{E}}^{T}\mathbf{h}\mathbf{T}_{\mathbf{E}}=\mathbf{h}\quad etc. \tag{63}$$

The variation of this functional Π_2 is:

$$\begin{aligned}&\delta\Pi_2(\delta\boldsymbol{\alpha},\delta\boldsymbol{\beta},\delta\boldsymbol{\gamma},\delta\mathbf{q}_{\mathbf{u}},\delta\mathbf{q}_{\boldsymbol{\varphi}},\delta\mathbf{q}_{\boldsymbol{\psi}})=\\&-\begin{Bmatrix}\delta\boldsymbol{\alpha}\\ \delta\boldsymbol{\beta}\\ \delta\boldsymbol{\gamma}\end{Bmatrix}^{T}\mathbf{H}\begin{Bmatrix}\boldsymbol{\alpha}\\ \boldsymbol{\beta}\\ \boldsymbol{\gamma}\end{Bmatrix}+\begin{Bmatrix}\delta\boldsymbol{\alpha}\\ \delta\boldsymbol{\beta}\\ \delta\boldsymbol{\gamma}\end{Bmatrix}^{T}\mathbf{G}\begin{Bmatrix}\mathbf{q}_{\mathbf{u}}\\ \mathbf{q}_{\boldsymbol{\varphi}}\\ \mathbf{q}_{\boldsymbol{\psi}}\end{Bmatrix}+\begin{Bmatrix}\delta\mathbf{q}_{\mathbf{u}}\\ \delta\mathbf{q}_{\boldsymbol{\varphi}}\\ \delta\mathbf{q}_{\boldsymbol{\psi}}\end{Bmatrix}^{T}\mathbf{G}^{T}\begin{Bmatrix}\boldsymbol{\alpha}\\ \boldsymbol{\beta}\\ \boldsymbol{\gamma}\end{Bmatrix}-\begin{Bmatrix}\delta\mathbf{q}_{\mathbf{u}}\\ \delta\mathbf{q}_{\boldsymbol{\varphi}}\\ \delta\mathbf{q}_{\boldsymbol{\psi}}\end{Bmatrix}^{T}\mathbf{F}\end{aligned} \tag{64}$$

For an arbitrary $\{\delta\boldsymbol{\alpha}\quad\delta\boldsymbol{\beta}\quad\delta\boldsymbol{\gamma}\}$, we have $\mathbf{H}\begin{Bmatrix}\boldsymbol{\alpha}\\ \boldsymbol{\beta}\\ \boldsymbol{\gamma}\end{Bmatrix}=\mathbf{G}\begin{Bmatrix}\mathbf{q}_{\mathbf{u}}\\ \mathbf{q}_{\boldsymbol{\varphi}}\\ \mathbf{q}_{\boldsymbol{\psi}}\end{Bmatrix}$, hence

$$\begin{Bmatrix}\boldsymbol{\alpha}\\ \boldsymbol{\beta}\\ \boldsymbol{\gamma}\end{Bmatrix}=\mathbf{H}^{-1}\mathbf{G}\begin{Bmatrix}\mathbf{q}_{\mathbf{u}}\\ \mathbf{q}_{\boldsymbol{\varphi}}\\ \mathbf{q}_{\boldsymbol{\psi}}\end{Bmatrix} \tag{65}$$

and for an arbitrary $\{\delta\mathbf{q}_{\mathbf{u}}\quad\delta\mathbf{q}_{\boldsymbol{\varphi}}\quad\delta\mathbf{q}_{\boldsymbol{\psi}}\}$, we have:

$$\mathbf{G}^{T}\begin{Bmatrix}\boldsymbol{\alpha}\\ \boldsymbol{\beta}\\ \boldsymbol{\gamma}\end{Bmatrix}=\mathbf{F} \tag{66}$$

Substituting eq. (65) into eq. (66) we get:

$$\mathbf{G}^{T}\mathbf{H}^{-1}\mathbf{G}\begin{Bmatrix}\mathbf{q}_{\mathbf{u}}\\ \mathbf{q}_{\boldsymbol{\varphi}}\\ \mathbf{q}_{\boldsymbol{\psi}}\end{Bmatrix}=\mathbf{K}\begin{Bmatrix}\mathbf{q}_{\mathbf{u}}\\ \mathbf{q}_{\boldsymbol{\varphi}}\\ \mathbf{q}_{\boldsymbol{\psi}}\end{Bmatrix}=\mathbf{F} \tag{67}$$

The element stiffness matrix then has the form:

$$\mathbf{K}=\begin{bmatrix}\mathbf{K}_{\mathbf{uu}} & \mathbf{K}_{\boldsymbol{u\varphi}} & \mathbf{K}_{\boldsymbol{u\psi}}\\ \mathbf{K}_{\boldsymbol{u\varphi}}^{\mathbf{T}} & -\mathbf{K}_{\boldsymbol{\varphi\varphi}} & -\mathbf{K}_{\boldsymbol{\varphi\psi}}\\ \mathbf{K}_{\boldsymbol{u\psi}}^{\mathbf{T}} & -\mathbf{K}_{\boldsymbol{\varphi\psi}}^{\mathbf{T}} & -\mathbf{K}_{\boldsymbol{\psi\psi}}\end{bmatrix}=\mathbf{G}^{T}\mathbf{H}^{-1}\mathbf{G} \tag{68}$$

We call this element "Hybrid/mixed finite element based on Atluri's variational principle" ("HMFEM-AVP") for MEE materials. Note that the compatibility between the independently assumed strain, electric and magnetic fields and those

derived from the primal variables is enforced by the variational principle of the functional Π_2. Since this element is based on multi-field variational principle and involves Lagrangian multipliers, it is plagued by LBB conditions (discussed in subsection 3.2.5), and its solvability, convergence and stability are not guaranteed. Also the element requires evaluation of two matrices (**H** and **G**) and inversion of the matrix **H**. Hence, it is computationally inefficient and expensive.

3.2.4 HMFEM using collocation method

Assuming independent strain, electric and magnetic fields, written in terms of undetermined parameters ($\boldsymbol{\alpha}, \boldsymbol{\beta}$ and $\boldsymbol{\gamma}$) as in eq. (52), the compatibility between these independently assumed fields and the strain, electric and magnetic fields derived from the displacement, electric and magnetic potential fields (the primal variables), as in eq. (38), can be enforced using several ways; for example, collocation at some cleverly chosen points. Because the collocation of these fields should be done in the local orthogonal coordinate system, if the shape of the element is not rectangular, we should first transform the components of the strain, electric and magnetic field vectors, derived from the primal fields, from the Cartesian coordinate system to the local orthogonal coordinate system according to eqs. (49), (50) and (51):

$$\begin{aligned}
&\hat{\varepsilon}^P = \mathbf{T}_{\boldsymbol{\varepsilon}}^{-1}\boldsymbol{\varepsilon}^{\mathbf{P}} = \mathbf{T}_{\boldsymbol{\varepsilon}}^{-1}\mathbf{B}_{\mathbf{u}}(\xi^{\gamma})\mathbf{q}_{\mathbf{u}} = \hat{\mathbf{B}}_{\mathbf{u}}(\xi^{\gamma})\mathbf{q}_{\mathbf{u}} \\
&-\hat{\mathbf{E}}^P = -\mathbf{T}_{\mathbf{E}}^{-1}\mathbf{E}^{\mathbf{P}} = \mathbf{T}_{\mathbf{E}}^{-1}\mathbf{B}_{\boldsymbol{\varphi}}(\xi^{\gamma})\mathbf{q}_{\boldsymbol{\varphi}} = \hat{\mathbf{B}}_{\boldsymbol{\varphi}}(\xi^{\gamma})\mathbf{q}_{\boldsymbol{\varphi}} \\
&-\hat{\mathbf{H}}^P = -\mathbf{T}_{\mathbf{H}}^{-1}\mathbf{H}^{\mathbf{P}} = \mathbf{T}_{\mathbf{E}}^{-1}\mathbf{B}_{\boldsymbol{\psi}}(\xi^{\gamma})\mathbf{q}_{\boldsymbol{\psi}} = \hat{\mathbf{B}}_{\boldsymbol{\psi}}(\xi^{\gamma})\mathbf{q}_{\boldsymbol{\psi}}
\end{aligned} \tag{69}$$

[Dong and Atluri (2011)] proved that in order for these elements to pass the patch test, the collocation should be done at Gauss quadrature points so that the compatibility is enforced in a weak sense. It is not necessary to collocate all the components at the same points. Which component is collocated at which points in the element, can be based on the judiciously chosen physical behavior of the element.

Now, for the 2D four-node quadrilateral element as illustrated in Figure 1, we collocate each of the normal strain field components at the 4 points of the 2×2 Gaussian points (points 5-8 in Figure 1), while collocate the shear strain at the center point (point 0 in Figure 1) to get:

$$\begin{aligned}
&\hat{\varepsilon}_i^{In}(\xi^{\gamma k}, \boldsymbol{\alpha}_i) = \hat{\varepsilon}_i^{P}(\xi^{\gamma k}, \mathbf{q}_{\mathbf{u}}) \\
&\mathbf{G_1}\boldsymbol{\alpha}_{\mathbf{I}} = \mathbf{M_1}\mathbf{q}_{\mathbf{u}}, \quad \mathbf{G_2}\boldsymbol{\alpha}_{\mathbf{II}} = \mathbf{M_2}\mathbf{q}_{\mathbf{u}}, \qquad \mathbf{G_3}\alpha_{\mathbf{III}} = \mathbf{M_3}\mathbf{q}_{\mathbf{u}}
\end{aligned} \tag{70}$$

where $\xi^{\gamma k}$ are the collocation points. Similarly, we collocate the components of the electric and magnetic fields at the 4 points of the 2×2 Gaussian points to get:

$$\begin{aligned}
&\hat{E}_i^{In}(\xi^{\gamma k}, \boldsymbol{\beta}_i) = \hat{E}_i^{P}(\xi^{\gamma k}, \mathbf{q}_{\boldsymbol{\varphi}}) \\
&\mathbf{G_4}\boldsymbol{\beta}_{\mathbf{I}} = \mathbf{M_4}\mathbf{q}_{\boldsymbol{\varphi}}, \quad \mathbf{G_5}\beta_{\mathbf{II}} = \mathbf{M_5}\mathbf{q}_{\boldsymbol{\varphi}}
\end{aligned} \tag{71}$$

$$\begin{array}{l} \hat{H}_i^{In}(\xi^{\gamma k}, \boldsymbol{\gamma}_i) = \hat{H}_i^{P}(\xi^{\gamma k}, \mathbf{q}_{\boldsymbol{\psi}}) \\ \mathbf{G_6}\boldsymbol{\gamma}_{\mathbf{I}} = \mathbf{M_6}\mathbf{q}_{\boldsymbol{\psi}}, \quad \mathbf{G_7}\boldsymbol{\gamma}_{\mathbf{II}} = \mathbf{M_7}\mathbf{q}_{\boldsymbol{\psi}} \end{array} \tag{72}$$

So the independently assumed strain, electric and magnetic fields are:

$$\hat{\boldsymbol{\varepsilon}}^{In} = \begin{Bmatrix} \hat{\varepsilon}^{In1} \\ \hat{\varepsilon}^{In3} \\ \hat{\varepsilon}^{In5} \end{Bmatrix} = \begin{bmatrix} \mathbf{A}_{\boldsymbol{\varepsilon}\mathbf{1}}(\xi^{\gamma}) & \mathbf{0} & \mathbf{0} \\ \mathbf{0} & \mathbf{A}_{\boldsymbol{\varepsilon}\mathbf{3}}(\xi^{\gamma}) & \mathbf{0} \\ \mathbf{0} & \mathbf{0} & \mathbf{A}_{\boldsymbol{\varepsilon}\mathbf{5}}(\xi^{\gamma}) \end{bmatrix} \begin{bmatrix} \mathbf{L_1} \\ \mathbf{L_2} \\ \mathbf{L_3} \end{bmatrix} \mathbf{q_u} = \mathbf{A}_{\boldsymbol{\varepsilon}}(\xi^{\gamma})\mathbf{L}\mathbf{q_u} \tag{73}$$

$$-\hat{\mathbf{E}}^{In} = \begin{Bmatrix} -\hat{E}^{In1} \\ -\hat{E}^{In3} \end{Bmatrix} = \begin{bmatrix} \mathbf{A_{E1}}(\xi^{\gamma}) & 0 \\ 0 & \mathbf{A_{E3}}(\xi^{\gamma}) \end{bmatrix} \begin{bmatrix} \mathbf{J}_1 \\ \mathbf{J}_2 \end{bmatrix} \mathbf{q}_{\varphi} = \mathbf{A_E}(\xi^{\gamma})\mathbf{J}\mathbf{q}_{\varphi} \tag{74}$$

$$-\hat{\mathbf{H}}^{In} = \begin{Bmatrix} -\hat{H}^{In1} \\ -\hat{H}^{In3} \end{Bmatrix} = \begin{bmatrix} \mathbf{A_{H1}}(\xi^{\gamma}) & 0 \\ 0 & \mathbf{A_{H3}}(\xi^{\gamma}) \end{bmatrix} \begin{bmatrix} \mathbf{V}_1 \\ \mathbf{V}_2 \end{bmatrix} \mathbf{q}_{\psi} = \mathbf{A_H}(\xi^{\gamma})\mathbf{J}\mathbf{q}_{\psi} \tag{75}$$

where

$$\mathbf{L_1} = \mathbf{G_1^{-1}M_1}, \quad \mathbf{L_2} = \mathbf{G_2^{-1}M_2}, \quad \mathbf{L_3} = \mathbf{G_3^{-1}M_3},$$

$$\mathbf{J_1} = \mathbf{G_4^{-1}M_4}, \quad \mathbf{J_2} = \mathbf{G_5^{-1}M_5}, \quad \mathbf{V_1} = \mathbf{G_6^{-1}M_6}, \quad \mathbf{V_2} = \mathbf{G_7^{-1}M_7}$$

Then we have to transform the strain, electric and magnetic field components from the local orthogonal coordinate system into the Cartesian coordinate system (only if the shape of the element is not rectangular):

$$\begin{array}{l} \boldsymbol{\varepsilon}^{In} = \mathbf{T}_{\boldsymbol{\varepsilon}}\hat{\boldsymbol{\varepsilon}}^{In} = \mathbf{T}_{\boldsymbol{\varepsilon}}\mathbf{A}_{\boldsymbol{\varepsilon}}(\xi^{\gamma})\mathbf{L}\mathbf{q_u} = \mathbf{B}^*_{\boldsymbol{\varepsilon}}\mathbf{q_u} \\ -\mathbf{E}^{In} = -\mathbf{T_E}\hat{\mathbf{E}}^{In} = \mathbf{T_E}\mathbf{A_E}(\xi^{\gamma})\mathbf{J}\mathbf{q}_{\boldsymbol{\varphi}} = \mathbf{B}^*_{\mathbf{E}}\mathbf{q}_{\boldsymbol{\varphi}} \\ -\mathbf{H}^{In} = -\mathbf{T_H}\hat{\mathbf{H}}^{In} = \mathbf{T_H}\mathbf{A_H}(\xi^{\gamma})\mathbf{V}\mathbf{q}_{\boldsymbol{\psi}} = \mathbf{B}^*_{\mathbf{H}}\mathbf{q}_{\boldsymbol{\psi}} \end{array} \tag{76}$$

where

$$\mathbf{B}^*_{\boldsymbol{\varepsilon}} = \mathbf{T}_{\boldsymbol{\varepsilon}}\mathbf{A}_{\boldsymbol{\varepsilon}}(\xi^{\gamma})\mathbf{L}, \quad \mathbf{B}^*_{\mathbf{E}} = \mathbf{T_E}\mathbf{A_E}(\xi^{\gamma})\mathbf{J}, \quad \mathbf{B}^*_{\mathbf{H}} = \mathbf{T_H}\mathbf{A_H}(\xi^{\gamma})\mathbf{V} \tag{77}$$

Using Π_1, the functional used to derive the irreducible or the primal element, we get the following after dropping the superscript i for simplicity:

$$\Pi_1 = \sum \left(\int_{\Omega} \left[\frac{1}{2} \begin{Bmatrix} \boldsymbol{\varepsilon}^{In} \\ -\mathbf{E}^{In} \\ -\mathbf{H}^{In} \end{Bmatrix}^T \begin{bmatrix} \mathbf{C} & \mathbf{e}^T & \mathbf{d}^T \\ \mathbf{e} & -\mathbf{h} & -\mathbf{g}^T \\ \mathbf{d} & -\mathbf{g} & -\boldsymbol{\mu} \end{bmatrix} \begin{Bmatrix} \boldsymbol{\varepsilon}^{In} \\ -\mathbf{E}^{In} \\ -\mathbf{H}^{In} \end{Bmatrix} - \bar{\mathbf{b}}^T\mathbf{u} + \overline{\rho_f}\varphi \right] d\Omega \right.$$
$$\left. - \int_{S_t} \bar{\mathbf{t}}^T\mathbf{u}\,ds - \int_{S_Q} \bar{Q}\varphi\,ds \right) \tag{78}$$

Equating the variation of the functional Π_1 to zero gives the finite element equation as in eq. (40), where the load vector $\mathbf{F}$ is exactly as expressed in eq. (42), while the stiffness matrix is defined as:

$$\begin{aligned}\mathbf{K} &= \begin{bmatrix} \mathbf{K_{uu}} & \mathbf{K}_{\boldsymbol{u\varphi}} & \mathbf{K}_{\boldsymbol{u\psi}} \\ \mathbf{K}^{\mathbf{T}}_{\boldsymbol{u\varphi}} & -\mathbf{K}_{\boldsymbol{\varphi\varphi}} & -\mathbf{K}_{\boldsymbol{\varphi\psi}} \\ \mathbf{K}^{\mathbf{T}}_{\boldsymbol{u\psi}} & -\mathbf{K}^{\mathbf{T}}_{\boldsymbol{\varphi\psi}} & -\mathbf{K}_{\boldsymbol{\psi\psi}} \end{bmatrix} \\ &= \begin{bmatrix} \mathbf{L}^T\left(\int_\Omega \mathbf{A}^T_{\boldsymbol{\varepsilon}}(\xi^\gamma)\mathbf{C}\mathbf{A}_{\boldsymbol{\varepsilon}}(\xi^\gamma)d\Omega\right)\mathbf{L} & \mathbf{L}^T\left(\int_\Omega \mathbf{A}^T_{\boldsymbol{\varepsilon}}(\xi^\gamma)\mathbf{e}^T\mathbf{A}_{\mathbf{E}}(\xi^\gamma)d\Omega\right)\mathbf{J} & \mathbf{L}^T\left(\int_\Omega \mathbf{A}^T_{\boldsymbol{\varepsilon}}(\xi^\gamma)\mathbf{d}^T\mathbf{A}_{\mathbf{H}}(\xi^\gamma)d\Omega\right)\mathbf{V} \\ \mathbf{J}^T\left(\int_\Omega \mathbf{A}^T_{\mathbf{E}}(\xi^\gamma)\mathbf{e}\mathbf{A}_{\boldsymbol{\varepsilon}}(\xi^\gamma)d\Omega\right)\mathbf{L} & -\mathbf{J}^T\left(\int_\Omega \mathbf{A}^T_{\mathbf{E}}(\xi^\gamma)\mathbf{h}\mathbf{A}_{\mathbf{E}}(\xi^\gamma)d\Omega\right)\mathbf{J} & -\mathbf{J}^T\left(\int_\Omega \mathbf{A}^T_{\mathbf{E}}(\xi^\gamma)\mathbf{g}^T\mathbf{A}_{\mathbf{H}}(\xi^\gamma)d\Omega\right)\mathbf{V} \\ \mathbf{V}^T\left(\int_\Omega \mathbf{A}^T_{\mathbf{H}}(\xi^\gamma)\mathbf{d}\mathbf{A}_{\boldsymbol{\varepsilon}}(\xi^\gamma)d\Omega\right)\mathbf{L} & -\mathbf{V}^T\left(\int_\Omega \mathbf{A}^T_{\mathbf{H}}(\xi^\gamma)\mathbf{g}\mathbf{A}_{\mathbf{E}}(\xi^\gamma)d\Omega\right)\mathbf{J} & -\mathbf{V}^T\left(\int_\Omega \mathbf{A}^T_{\mathbf{H}}(\xi^\gamma)\boldsymbol{\mu}\boldsymbol{A}_{\mathbf{H}}(\xi^\gamma)d\Omega\right)\mathbf{V} \end{bmatrix} \end{aligned} \tag{79}$$

where we used the identities in eq. (63).

We will call this element "Hybrid/mixed finite element with collocation" ("HMFEM-C"). The unlocked nature of this HMFEM-C element that improved the accuracy of the mechanical displacements in [Dong and Atluri (2011); Bishay and Atluri (2012)] is expected to improve the accuracy of the electric and magnetic potentials as well because of the electro-elastic and magneto-elastic couplings of the MEE materials nature. Note that in developing this element we only used the simple irreducible version of the variational principle used commonly with the primal finite elements not the multi-field variational principle that always result in the presence of Lagrangian multiplier which plague the LBB conditions.

3.2.5 On LBB conditions

The hybrid/mixed elements that are based on multi-field variational principles, such as "HMFEM-AVP", always involove Lagrangian multipliers (the term $\{\boldsymbol{\sigma} \quad \mathbf{D} \quad \mathbf{B}\}$ in eq. (28)). Babuska (1973) and Brezzi (1974) studied general saddle-point problems or problems involving Lagrangian multipliers, and established the so-called LBB conditions. Inability to satisfy LBB conditions in general would plague the solvability and stability of hybrid/mixed finite element equations. These LBB conditions exist only when using multi-field variational principles, where Lagrangian multipliers are involved.

The solvability and stability of HMFEM-AVP is thus governed by the LBB conditions. The LBB conditions consists of two conditions, the first is always satisfied if we have a positive-definite material properties. The second condition is thus the key condition governing the performance of hybrid/mixed finite element method. This condition has the following strong physical meaning: "for every non-rigid

body displacement mode in each element, there should be at least one independently assumed strain mode, so that the derived 'mixed strain energy' is positive". For MEE materials, by "displacement", we mean the primal variables "displacements and electric and magnetic potentials", and by "strain", we mean "strain, electric and magnetic fields". This condition is frequently considered as free of zero-energy/kinematic/spurious modes in a mechanics point of view. An equivalent condition to the second LBB condition is the condition of rank-sufficiency:

$$rank(\mathbf{G}) = n_{dof} - r \tag{80}$$

where $\mathbf{G}$ is defined as in eq. (62), n_{dof} is the number of degrees of freedom and r is the number of rigid-body modes. The necessary condition of selecting at least $n_{dof} - r$ independent strain modes and ensure eq. (80) beforehand in the element formulation level is difficult. Atluri and his co-workers in [Punch and Atluri (1984); Rubinstein *et al.* (1984)] used a sophisticated group theory to develop guidelines for selecting least-order stress interpolations, from which stable and invariant finite elements satisfying LBB conditions can be formulated. It was the first time for the symmetric group theory to be utilized to prevent element rank deficiency. However its application in engineering is limited by the mathematical sophistication and complexity of group theory. [Pian and Chen (1983)] also proposed to choose stress interpolations by matching each stress/strain mode to each of the stress/strain modes derived from non-rigid-body displacement modes to suppress zero-energy modes, but they did not consider the invariance of the derived elements. No matter which method one chooses to use, we see that because of LBB conditions, the independent fields cannot be arbitrarily chosen. Careful and complicated analysis has to be conducted in order to ensure the stability of the solution, which is especially complicated for three-dimensional and higher-order elements.

The new H/M element ("HMFEM-C") presented here uses the primitive field variational principle; hence do not involve Lagrangian multipliers, and avoids the LBB conditions completely. So for the numerical examples to be presented in section 5 of this paper, we will only consider "HMFEM-C" elements.

3.3 Node-wise material properties

When dealing with functionally graded materials, nodal-defined material properties can be used to provide smooth variation of the material properties as required by the grading function, and avoid jumps in the material properties between the elements. Hence, the material properties in each element can be written using the

shape function representation that allows specifying nodal material properties:

$$\begin{aligned} C_{ij} &= \sum_n C_{ij}^{(n)} N_C^{(n)}(\xi^\gamma), \quad e_{ij} = \sum_n e_{ij}^{(n)} N_e^{(n)}(\xi^\gamma), \quad d_{ij} = \sum_n d_{ij}^{(n)} N_d^{(n)}(\xi^\gamma) \\ h_{ij} &= \sum_n h_{ij}^{(n)} N_h^{(n)}(\xi^\gamma), \quad \mu_{ij} = \sum_n \mu_{ij}^{(n)} N_\mu^{(n)}(\xi^\gamma), \quad g_{ij} = \sum_n g_{ij}^{(n)} N_g^{(n)}(\xi^\gamma) \end{aligned} \tag{81}$$

In vector and matrix notation:

$$\begin{aligned} \mathbf{C} &= \mathbf{N_C}(\xi^\gamma)\mathbf{Q_C}, \quad \mathbf{e} = \mathbf{N_e}(\xi^\gamma)\mathbf{Q_e}, \quad \mathbf{d} = \mathbf{N_d}(\xi^\gamma)\mathbf{Q_d} \\ \mathbf{h} &= \mathbf{N_h}(\xi^\gamma)\mathbf{Q_h}, \quad \boldsymbol{\mu} = \mathbf{N_\mu}(\xi^\gamma)\mathbf{Q_\mu}, \quad \mathbf{g} = \mathbf{N_g}(\xi^\gamma)\mathbf{Q_g} \end{aligned} \tag{82}$$

where $\mathbf{Q_C}, \mathbf{Q_e}, \mathbf{Q_d}, \mathbf{Q_h}, \mathbf{Q_\mu}$ and $\mathbf{Q_g}$ are the nodal elastic stiffness, piezoelectric, piezomagnetic, dielectric, magnetic permeability and magnetoelectric material matrices, and $\mathbf{N_C}(\xi^\gamma), \mathbf{N_e}(\xi^\gamma), \mathbf{N_d}(\xi^\gamma), \mathbf{N_h}(\xi^\gamma), \mathbf{N_\mu}(\xi^\gamma)$, and $\mathbf{N_g}(\xi^\gamma)$ are the associated shape functions. This representation allows each node in a single element to have its own material properties and is to be used in the stiffness matrices for "PFEM", "HMFEM-AVP" and "HMFEM-C" (eqs. (41), (68) and (79) respectively) when dealing with functionally-graded materials.

3.4 Conditioning of system matrices

The finite element global system of equations to be solved using any of the previously presented elements is ill-conditioned because the stiffness matrix contains the material elastic stiffness matrix $\mathbf{C}$ in the $\mathbf{K_{uu}}$ part and also contains the dielectric material matrix $\mathbf{h}$ in the $\mathbf{K_{\varphi\varphi}}$ part. The numerical values of the components of $\mathbf{C}$ are as large as 10^{10}, and that of $\mathbf{h}$ are as small as 10^{-9}. Hence the ratio is as large as 10^{19}, and this makes the global stiffness matrix ill-conditioned. To improve the conditioning we can use the following matrix instead of that of eq. (7):

$$\begin{Bmatrix} \hat{\boldsymbol{\sigma}} \\ \hat{\mathbf{D}} \\ \hat{\mathbf{B}} \end{Bmatrix} = \begin{bmatrix} \hat{\mathbf{C}} & \hat{\mathbf{e}}^T & \hat{\mathbf{d}}^T \\ \hat{\mathbf{e}} & -\hat{\mathbf{h}} & -\hat{\mathbf{g}}^T \\ \hat{\mathbf{d}} & -\hat{\mathbf{g}} & -\hat{\boldsymbol{\mu}} \end{bmatrix} \begin{Bmatrix} \boldsymbol{\varepsilon} \\ -\hat{\mathbf{E}} \\ -\hat{\mathbf{H}} \end{Bmatrix} \tag{83}$$

where $\hat{\sigma}_i = \frac{\sigma_i}{\tilde{c}}$, $\hat{D}_i = \frac{D_i}{\tilde{e}}$, $\hat{B}_i = \frac{B_i}{\tilde{d}}$, $\hat{E}_i = \frac{E_i \tilde{e}}{\tilde{c}}$, $\hat{H}_i = \frac{H_i \tilde{d}}{\tilde{c}}$ and $\hat{C}_{ij} = \frac{C_{ij}}{\tilde{c}}$,
$\hat{e}_{ij} = \frac{e_{ij}}{\tilde{e}}$, $\hat{h}_{ij} = \frac{h_{ij}\tilde{c}}{\tilde{e}^2}$, $\hat{d}_{ij} = \frac{d_{ij}}{\tilde{d}}$, $\hat{g}_{ij} = \frac{g_{ij}\tilde{c}}{\tilde{e}\tilde{d}}$, $\hat{\mu}_{ij} = \frac{\mu_{ij}\tilde{c}}{\tilde{d}^2}$.
From eqs. (5) and (6), we also have $\hat{\varphi} = \frac{\varphi\tilde{e}}{\tilde{c}}$, $\hat{\psi} = \frac{\psi\tilde{d}}{\tilde{c}}$.
Here we can select $\tilde{c} = C_{11}$, $\tilde{e} = e_{33}$ and $\tilde{d} = d_{33}$.

Hence, the stiffness matrix for PFEM, for example, will have the form:

$$\hat{\mathbf{K}} = \begin{bmatrix} \hat{\mathbf{K}}_{\mathbf{uu}} & \hat{\mathbf{K}}_{\boldsymbol{u\varphi}} & \hat{\mathbf{K}}_{\boldsymbol{u\psi}} \\ \hat{\mathbf{K}}^{\mathbf{T}}_{\boldsymbol{u\varphi}} & -\hat{\mathbf{K}}_{\boldsymbol{\varphi\varphi}} & -\hat{\mathbf{K}}_{\boldsymbol{\varphi\psi}} \\ \hat{\mathbf{K}}^{\mathbf{T}}_{\boldsymbol{u\psi}} & -\hat{\mathbf{K}}^{\mathbf{T}}_{\boldsymbol{\varphi\psi}} & -\hat{\mathbf{K}}_{\boldsymbol{\psi\psi}} \end{bmatrix}$$
$$= \begin{bmatrix} \int_{\Omega} \mathbf{B}_{\mathbf{u}}^T \hat{\mathbf{C}} \mathbf{B}_{\mathbf{u}} d\Omega & \int_{\Omega} \mathbf{B}_{\mathbf{u}}^T \hat{\mathbf{e}}^T \mathbf{B}_{\boldsymbol{\varphi}} d\Omega & \int_{\Omega} \mathbf{B}_{\mathbf{u}}^T \hat{\mathbf{d}}^T \mathbf{B}_{\boldsymbol{\psi}} d\Omega \\ \int_{\Omega} \mathbf{B}_{\boldsymbol{\varphi}}^T \hat{\mathbf{e}} \mathbf{B}_{\mathbf{u}} d\Omega & -\int_{\Omega} \mathbf{B}_{\boldsymbol{\varphi}}^T \hat{\mathbf{h}} \mathbf{B}_{\boldsymbol{\varphi}} d\Omega & -\int_{\Omega} \mathbf{B}_{\boldsymbol{\varphi}}^T \hat{\mathbf{g}}^T \mathbf{B}_{\boldsymbol{\psi}} d\Omega \\ \int_{\Omega} \mathbf{B}_{\boldsymbol{\psi}}^T \hat{\mathbf{d}} \mathbf{B}_{\mathbf{u}} d\Omega & -\int_{\Omega} \mathbf{B}_{\boldsymbol{\psi}}^T \hat{\mathbf{g}} \mathbf{B}_{\boldsymbol{\varphi}} d\Omega & -\int_{\Omega} \mathbf{B}_{\boldsymbol{\psi}}^T \hat{\mu} \mathbf{B}_{\boldsymbol{\psi}} d\Omega \end{bmatrix} \tag{84}$$

And the system to be solved will be:

$$\hat{\mathbf{K}}\hat{\mathbf{q}} = \hat{\mathbf{F}} \tag{85}$$

where

$$\hat{\mathbf{F}} = \begin{Bmatrix} \hat{\mathbf{F}}_{\mathbf{u}} \\ \hat{\mathbf{F}}_{\boldsymbol{\varphi}} \\ \mathbf{0} \end{Bmatrix}, \qquad \hat{\mathbf{F}}_{\mathbf{u}} = \frac{\mathbf{F}_{\mathbf{u}}}{\tilde{c}}, \;\; \hat{\mathbf{F}}_{\boldsymbol{\varphi}} = \frac{\mathbf{F}_{\boldsymbol{\varphi}}}{\tilde{e}} \tag{86}$$

$\hat{\mathbf{q}} = \begin{Bmatrix} \mathbf{q}_{\mathbf{u}} & \hat{\mathbf{q}}_{\boldsymbol{\varphi}} & \hat{\mathbf{q}}_{\boldsymbol{\psi}} \end{Bmatrix}^T$ and $\hat{\mathbf{q}}_{\boldsymbol{\varphi}} = \frac{\mathbf{q}_{\boldsymbol{\varphi}} \tilde{e}}{\tilde{c}}$, $\hat{\mathbf{q}}_{\boldsymbol{\psi}} = \frac{\mathbf{q}_{\boldsymbol{\psi}} \tilde{d}}{\tilde{c}}$.
So, we solve the system (85) for $\hat{\mathbf{q}}$ from which we get $\mathbf{q}_{\mathbf{u}}$, $\mathbf{q}_{\boldsymbol{\varphi}} = \frac{\hat{\mathbf{q}}_{\boldsymbol{\varphi}} \tilde{c}}{\tilde{e}}$ and $\mathbf{q}_{\boldsymbol{\psi}} = \frac{\hat{\mathbf{q}}_{\boldsymbol{\psi}} \tilde{c}}{\tilde{d}}$.

4 Magnetoelectric (ME) voltage coefficients

A general 2D computer code was developed to deal with magneto-electro-elastic materials or pure PE and PM layers using the previously presented elements and the node-wise material properties for functionally graded piezoelectric-piezomagnetic (PE-PM) composites. In this paper, the main application of the developed finite element model is to investigate the effect of the layers' thicknesses (or the volume fraction of the PE phase, to be defined in eq. (94)) and the mechanical boundary conditions on the magnetoelectric coupling in PE-PM composites. Hence, we define three configurations or modes for measuring the ME voltage coefficients:

1. Longitudinal or out-of-plane mode: Both the poling direction $\boldsymbol{P}_e$ in the PE layer and the magnetic bias direction $\boldsymbol{P}_m$ in the PM layer are vertically upward (through the layer thickness) and the applied magnetic field in the PM layer as well as the measured electric field in the PE layer is directed vertically through the thickness.

2. Transverse mode: the magnetic bias direction $\boldsymbol{P}_m$ in the PM layer is parallel to the layer plan, and so is the applied magnetic field. While the poling direction $\boldsymbol{P}_e$ in the PE layer as well as the measured electric field is vertically through the thickness.

3. In-plane mode: the magnetic bias direction $\boldsymbol{P}_m$ in the PM layer and the applied magnetic field as well as the poling direction $\boldsymbol{P}_e$ in the PE layer, and the measured electric field are all directed in-plane.

These three modes are shown in Figure 2.

Accordingly, we have three ME voltage coefficients, one for each mode. Here we have to clarify the difference between the ME voltage coefficient and the homogenized ME voltage coefficient [Chang and Carman (2008)]. The ME voltage coefficient is defined as:

$$\alpha'_{ij} = \frac{\bar{E}_i}{\bar{H}_j} \tag{87}$$

where $\bar{H}_j$ is the average applied magnetic field in the piezomagnetic phase while $\bar{E}_i$ is the average electric field in the piezoelectric phase only.

However, in order to compare the ME voltage coefficients with the monolithic systems, homogenized ME voltage coefficient is used where $\bar{E}_i$ is the measured electric field in the whole sample rather than just the piezoelectric layer. In this study, we use the homogenized ME voltage coefficient for the out-of plane and transverse modes where the electric field is measured vertically in the thickness direction. This is consistent with previous presentations [Bichurin *et al.* (2003); Chang and Carman (2008); Pan and Wang (2009); Sladek *et al.* (2012 a, b)].

The average intensity of the electric field $\bar{E}_i$ is defined for the composite plate as:

$$\bar{E}_i = \frac{1}{S}\int_S E_i(x_1, x_3)dS \tag{88}$$

where S is the surface of the two-layered composite in the $x_1 - x_3$ plane. The average magnetic field intensity vector is defined similarly. We will either specify a value for the electric potential on the bottom surface of the composite or on the left surface of the PE layer. This value is taken as zero here to set these surfaces as the electric ground of the composite. In the considered samples with $t_e + t_m = t \ll L$, the average electric fields can be assessed as:

$$\begin{aligned} \bar{E}_3 &= \frac{\bar{\varphi}_{low} - \bar{\varphi}_{up}}{t_e + t_m} = -\frac{\bar{\varphi}_{up}}{t} \text{ V / m}, \\ \bar{E}_1 &= \frac{\bar{\varphi}_{left} - \bar{\varphi}_{right}}{L} = -\frac{\bar{\varphi}_{right}}{L} \quad \text{V / m} \end{aligned} \tag{89}$$

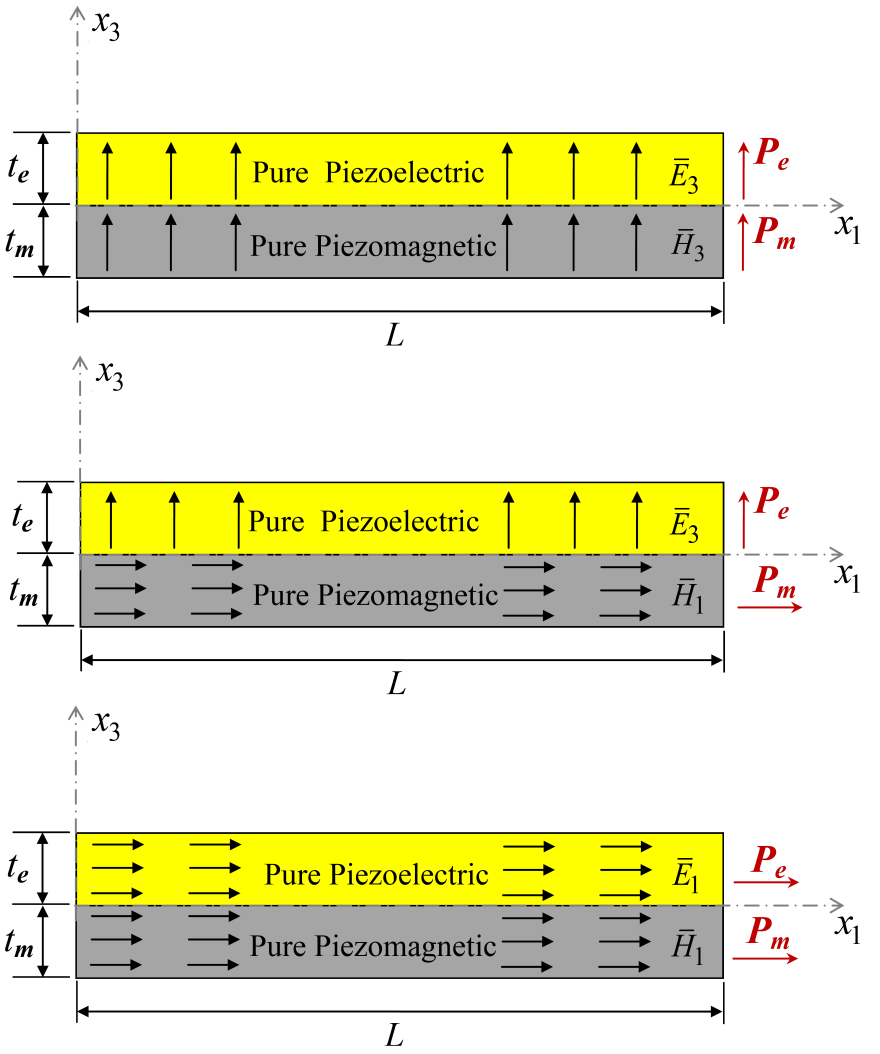

Figure 2: (upper): Longitudinal or out-of-plane mode, (middle): Transverse mode, (lower): In-plane mode. (polling and magnetic bias directions are indicated by the red arrows beside each layer)

where $\bar{\varphi}_{low}$ and $\bar{\varphi}_{left}$ are the specified electric potential at the bottom surface of the whole composite and on the left surface of the PE layer only, while $\bar{\varphi}_{up}$ and $\bar{\varphi}_{right}$ are the average electric potential at the top surface of the whole composite and on the right surface of the PE layer only. t_e, t_m and L are the PE and PM layer thicknesses, and the length of the composite. $t = t_e + t_m$ is the total thickness of the

composite. $\bar{\varphi}_{low} = \bar{\varphi}_{left} = 0$.

For a constant magnetic field, $\bar{H}_3$, applied vertically in the PM layer, the homogenized out-of-plane magnetoelectric (ME) voltage coefficient is defined as:

$$\alpha'_{33} = \frac{\bar{E}_3}{\bar{H}_3} = -\frac{\bar{\varphi}_{up}}{\bar{H}_3 t} \quad \text{V / A} \tag{90}$$

For a constant magnetic field, $\bar{H}_1$, applied horizontally in the PM layer, the homogenized transverse magnetoelectric (ME) voltage coefficient is defined as:

$$\alpha'_{31} = \frac{\bar{E}_3}{\bar{H}_1} = -\frac{\bar{\varphi}_{up}}{\bar{H}_1 t} \quad \text{V / A} \tag{91}$$

and finally, the in-plane magnetoelectric (ME) voltage coefficient is written as:

$$\alpha'_{11} = -\frac{\bar{E}_1}{\bar{H}_1} = \frac{\bar{\varphi}_{right}}{\bar{H}_1 L} \quad \text{V / A} \tag{92}$$

(The negative sign is used to keep α'_{11} positive).

In order to check the effect of the layers' thicknesses on the ME voltage coefficients, we define V_f, the volume fraction of the piezoelectric phase in the PE-PM composite as:

$$V_f = \frac{t_e}{t_e + t_m} = \frac{t_e}{t} \tag{93}$$

In the numerical examples to be presented in the next section, the total thickness of composite, $t = t_e + t_m$, is kept constant, while the volume fraction V_f is changed from 0 (pure piezomagnetic phase; $\alpha'_{33} = \alpha'_{31} = \alpha'_{11} = 0$ in this case) to 1 (pure piezoelectric phase; $\alpha'_{33} = \alpha'_{31} = \alpha'_{11} = 0$ in this case as well) and the three ME voltage coefficients are calculated.

To apply constant magnetic field, $\bar{H}_3$, in the PM layer, we specify a value for the magnetic potential on the bottom surface of the composite, $\bar{\psi}_{low}$, and we take the top surface of the composite to be the magnetic ground ($\bar{\psi}_{up} = 0$). Using the definition of the average vertical magnetic field:

$$\bar{H}_3 = \frac{\bar{\psi}_{low} - \bar{\psi}_{up}}{t_m} = \frac{\bar{\psi}_{low}}{t_m} \quad \text{A / m}, \tag{94}$$

we get the prescribed magnetic potential on the lower boundary, for a fixed value of $\bar{H}_3$, as a function of V_f:

$$\bar{\psi}_{low} = \bar{H}_3 t\,(1 - V_f) \quad \text{A} \tag{95}$$

Similarly, to apply constant magnetic field, $\bar{H}_1$, in the PM layer, we specify a value for the magnetic potential on the left surface of the composite, $\bar{\psi}_{left}$, and we take the right surface of the composite to be the magnetic ground ($\bar{\psi}_{right} = 0$). Then the average horizontal magnetic field is:

$$\bar{H}_1 = \frac{\bar{\psi}_{left} - \bar{\psi}_{right}}{L} = \frac{\bar{\psi}_{left}}{L} \quad \text{A / m} \tag{96}$$

The prescribed magnetic potential on the right boundary, $\bar{\psi}_{left}$, is not a function of V_f and can be obtained directly from eq. (96).

The electric and magnetic essential BCs for the three modes of the ME voltage coefficient (out-of-plane, transverse and in-plane) are shown in Figure 3. The top surface of the PM layer and the bottom surface of the PE layer are perfectly bonded and both magnetic flux and electrical displacements are unknown there.

5 Numerical experiments and results

Since the HMFEM-AVP element is plagued by LBB conditions and less efficient than HMFEM-C, the latter only will be used in the numerical experiments. These HMFEM-C elements proved superior performance over the primal elements especially when the structure is loaded in bending or shear.

In this section, in order to validate our developed computer code and check the performance of the new magneto-electro-elastic hybrid/mixed finite elements, we consider the patch test first, and then we compare the accuracy of the developed HMFEM-C element with that of the PFEM in a problem of a cantilevered MEE beam subjected to end shear load. In these experiments, we calculate the error relative to the results of the analytical solutions in [Jiang and Ding (2004)]. Using the developed and validated code, we present some numerical experiments on bi-layered piezoelectric-piezomangetic composites with/without functionally graded layers, and single-layer functionally graded magneto-electro-elastic material with pure piezomangetic properties at its bottom surface and pure piezoelectric properties at its top surface. Several mechanical boundary conditions will be considered. Magnetic as well as mechanical loads are applied. The effect of the volume fraction of the piezoelectric phase on the various magnetoelectric (ME) voltage coefficients is investigated as well as the effect of the grading functions in the functionally graded composites. The material used in the code validation examples is the magneto-electro-elastic material considered in the paper of [Jiang and Ding (2004)] whose properties are shown in Table 1 with plane stress assumption. While in the other numerical experiments, the piezoelectric material used is PZT-5A while the piezomagnetic material is $CoFe_2O_4$. The material constants for both, with plane strain assumption, are presented in Table 1 as well.

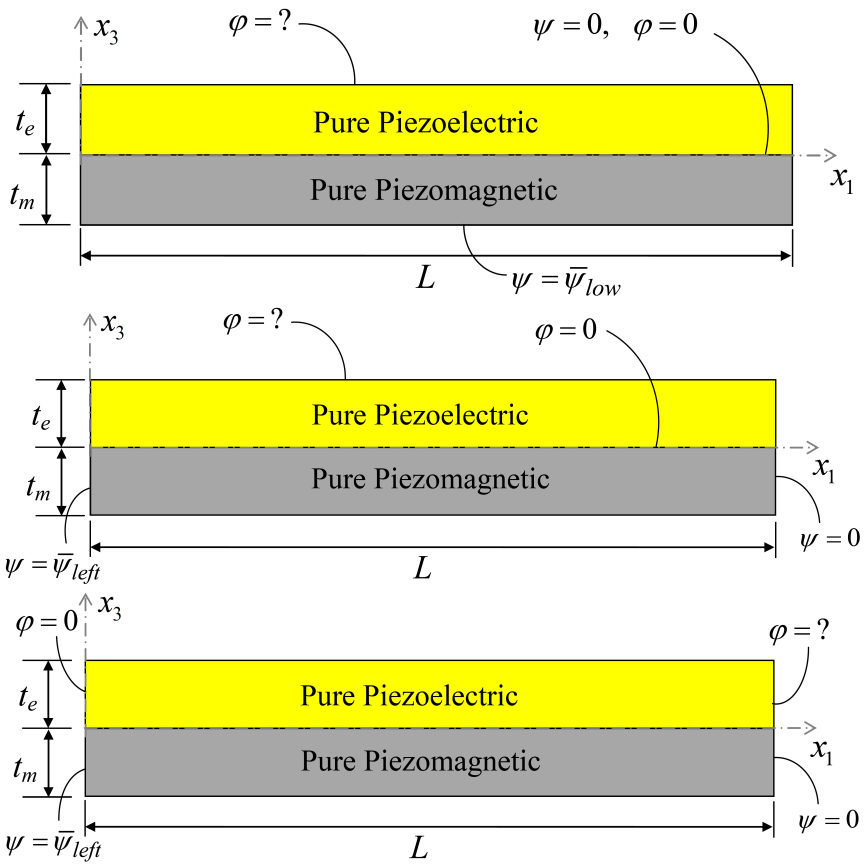

Figure 3: The considered electric and magnetic BCs for the three modes of the ME voltage coefficient: (upper) out-of-plane, (middle) transverse, (lower) in-plane

5.1 Code validation

5.1.1 Patch test

Consider a patch of a rectangular shape as shown in Figure 4. The body is fixed at its left edge and a uniformly distributed load of magnitude P is applied on its right edge. The middle point in the left edge is considered as the electric and magnetic ground. Plane stress assumption is used. The material properties are that presented in Table 1 as MEE (Jiang). Here we select $L = 0.3$ m, $W = 0.15$ m, and $P = 500$ Pa.

We compare the finite element results at point "A" (the middle point on the upper edge) with that of the analytical solution presented in [Jiang and Ding (2004)]. The analytical solution at point "A" is: $u_1 = 0.6016 \times 10^{-8}$m, $u_3 = -0.1130 \times 10^{-8}$m,

Table 1: Material constants for PZT-5A piezoelectric material (plane strain), $CoFe_2O_4$ piezomagnetic material (plane strain) and MEE material (plane stress) used by Jaing and Ding (2004) [C_{ij} in 10^9 Pa, e_{ij} in C/m^2, d_{ij} in N/Am, h_{ij} in 10^{-8} C/Vm, g_{ij} in 10^{-12} Ns/VC, and μ_{ij} in 10^{-4} Ns^2/C^2]

Material	C_{11}	C_{13}	C_{33}	C_{44}	e_{15}	e_{31}	e_{33}	h_{11}
PZT-5A	99.2	50.778	86.859	21.1	12.332	-7.209	15.118	1.53
$CoFe_2O_4$	286	170.5	269.5	45.3	0	0	0	-
MEE (Jiang)	130.28	41.819	125.35	43	11.6	-2.359	20.6675	1.12
Material	h_{33}	d_{15}	d_{31}	d_{33}	μ_{11}	μ_{33}	g_{11}	g_{33}
PZT-5A	1.5	0	0	0	-	-	0	0
$CoFe_2O_4$	-	550	580.3	699.7	5.90	1.57	0	0
MEE (Jiang)	1.2717	550	311.125	427.029	0.05	0.1	5	-1.5378

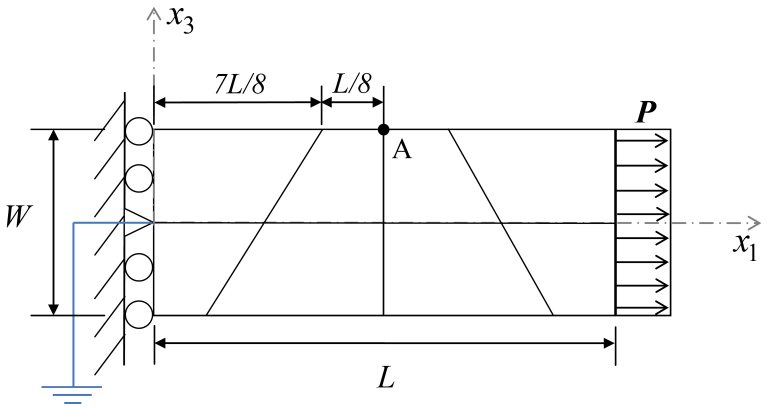

Figure 4: The considered patch test

$\varphi = -2.5082$V, and $\psi = 0.0604$ A. The finite element mesh considered here is 2 $\times$ 4 distorted elements as shown in the figure. The percentage error in the different variables for the two considered element types is presented in Table 2.

Table 2: Error percent for the different variables at point "A" in the constant stress patch test

	u_1	u_3	φ	ψ
PFEM	-0.1237 $\times$ 10^{-12}	0	-0.0531 $\times$ 10^{-12}	-0.3676 $\times$ 10^{-12}
HMFEM-C	0.0784 $\times$ 10^{-11}	0.3805 $\times$ 10^{-11}	0.0691 $\times$ 10^{-11}	-0.0356 $\times$ 10^{-11}

The error at all of the nodes defined by:

$$Error\ \% = \frac{\|\mathbf{q} - \mathbf{q}^{exact}\|}{\|\mathbf{q}^{exact}\|} \times 100 \tag{97}$$

for the two considered element types is: 1.7948×10^{-13} for PFEM and 5.2639×10^{-13} for HMFEM-C. It is clear that the error is very small for both elements; hence both element types pass the constant stress patch test.

5.1.2 Cantilever beam with end shear load

Jiang and Ding (2004) presented the analytical solutions of 2D magneto-electro-elastic beams with different loading and boundary conditions by expressing all the variables in terms of four harmonic displacement functions. Here we consider the problem of a cantilever beam subjected to end shear as shown in Figure 5. The electric and magnetic grounds are selected to be the middle point of the left edge. The geometric properties of the beam are: length L = 0.3 m, width W = 0.02 m, while the material properties are that presented in Table 1 as MEE (Jiang). Plane stress assumption is used. The applied shear load P = 50 N.

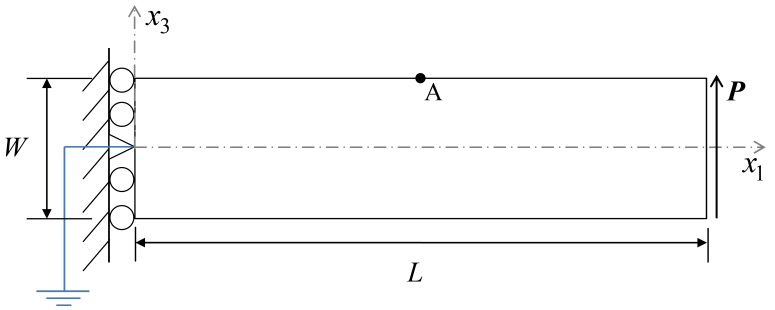

Figure 5: Cantilever beam subjected to end shear force

The analytical solution at point "A" is: $u_1 = -2.0281 \times 10^{-7}$m, $u_3 = 1.6934 \times 10^{-6}$m, $\varphi = 7.1244$V, and $\psi = 0.2665$ A, Meshing the body using 2×4, 4×8 and 6×12 elements, we get the results shown in Table 3 for the error percentage in primal variables at point "A" for the PFEM and HMFEM-C.

It is very clear that HMFEM-C is much more accurate than PFEM, not only in the mechanical displacements, but also in the electric and magnetic potentials. For HMFEM-C, with 4 elements in the width direction, it is only 8 elements required in the length direction to get error percent less than 1 %. However for the PFEM elements, even with 60 elements in the length direction, we cannot get this low error percentage.

Table 3: Error percentage at point "A"

	Mesh	2×4	4×8	6×12
PFEM	u_1	82.9209	54.8028	34.9779
	u_3	83.1705	54.9311	35.0154
	φ	43.0648	28.5710	18.2948
	ψ	27.8488	18.2948	12.2599
HMFEM-C	u_1	1.0306	0.1462	0.0323
	u_3	3.4236	0.6413	0.1145
	φ	3.1727	0.5268	0.1583
	ψ	1.9288	0.0917	0.0549

5.2 Bi-layered piezoelectric-piezomangetic composites

In dealing with PE-PM and functionally graded PE-PM composites in this section and the next two sections, four mechanical boundary condition cases are considered. These BC cases are shown in Figure 6. BC1 is a composite with its bottom surface totally clamped, while in BC2 the bottom surface is fixed only in the vertical direction (the horizontal displacement is zero only at the lower left edge). BC3 is a composite with its left surface fixed only in the horizontal direction, while BC4 has the lower left edge totally fixed, and the upper left edge is allowed to move in the vertical direction only (so the mechanical rigid body motions are prevented). All other surfaces are traction free with vanishing electric displacement and magnetic induction.

The effect of applying mechanical loads in addition to the applied magnetic field will also be investigated. The considered load cases are as follows: for all BCs, a uniformly distributed stress applied on the top surface of the composite is considered, while only for BC3 and BC4, a uniformly distributed stress, concentrated shear and concentrated moment applied on the right surface are also considered. All these cases are shown in Figure 7.

The following geometrical values for the two-layered composite are considered in the numerical analysis: length $L = 16$ mm, and total thickness of $t = t_e + t_m = 2$ mm. For the upper layer with pure piezoelectric properties we have considered PZT-5A material, while the lower layer is a pure piezomagnetic layer having the properties of $CoFe_2O_4$ material. The material properties are shown in Table 1.

A magnetic field, $\bar{H}_3 = -100$ A / m, is applied in the PM layer for the out-of-plane mode, hence; the specified magnetic potential at the bottom surface is calculated through equation (95), $\bar{\psi} = \bar{\psi}_{low} = \bar{H}_3 t\,(1 - V_f) = -0.2\,(1 - V_f)$ A. Similarly, for the transverse and in-plane modes, a magnetic field, $\bar{H}_1 = -100$ A / m, is applied

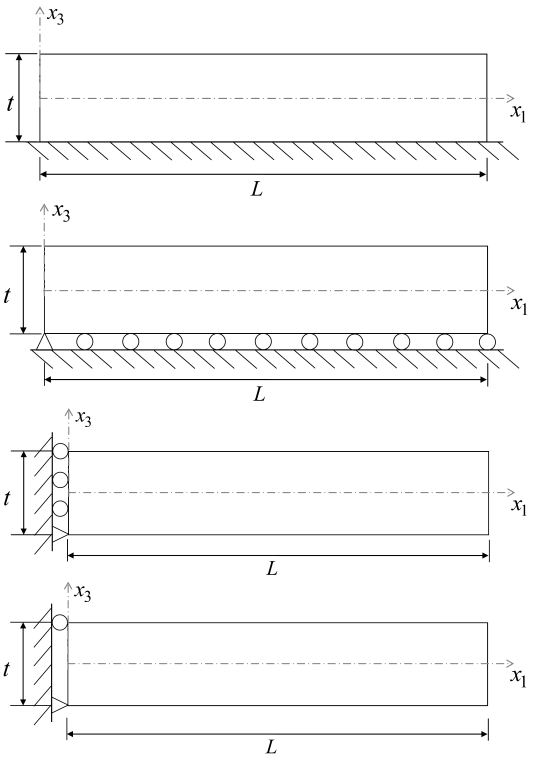

Figure 6: The considered mechanical BCs: (upper left) BC1: Clamped lower surface, (upper right) BC2: fixed lower surface, (lower left) BC3: fixed left surface, (lower right) BC4: only 2 points fixed on the left surface

in the PM layer and hence the prescribed magnetic potential at the right surface is calculated through equation (96), $\bar{\psi} = \bar{\psi}_{left} = \bar{H}_1 L = -1.6$ A.

A finite element mesh of 8 HMFEM-C elements in the thickness direction and 96 elements in the length direction is used. The results are verified with the results presented in [Sladek *et al.* (2012 a,b)]. The average electric potential on the upper surface of the PE layer, $\bar{\varphi}_{up}$, is calculated for the out-of-plane and transverse modes, and on the right surface of the PE layer, $\bar{\varphi}_{right}$, for the in-plane mode. Then, the three ME voltage coefficients are calculated using eqs. (90) to (92).

When only magnetic loading is applied in the PM layer without any mechanical loads, the variation of the three ME voltage coefficients as a function of the volume fraction of the piezoelectric phase is shown in Figure 8 for the four considered boundary conditions (illustrated in Figure 6).

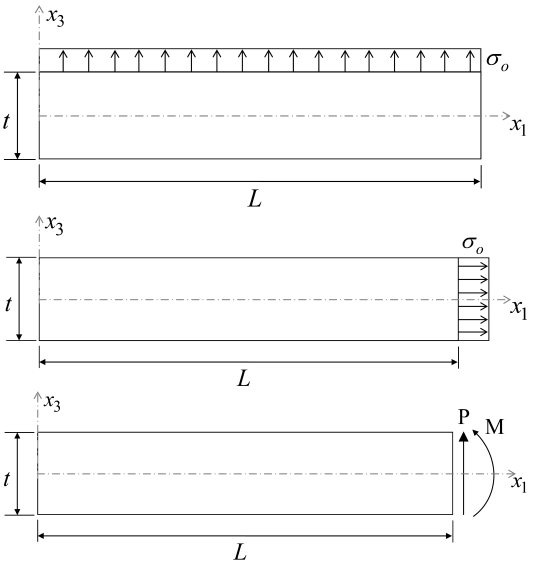

Figure 7: The considered applied mechanical loads: (upper) uniformly distributed load on the top surface for all BCs, (lower) uniformly distributed load, concentrated shear and concentrated moment on the right surface, only for BCs 3 and 4

It can be seen that: (1) for all the considered BCs, the in-plane ME voltage coefficient α'_{11} is the largest, followed by the transverse, α'_{31}, then the out-of-plane ME voltage coefficient, α'_{33}, (2) all the three ME voltage coefficients for BC2 (fixed bottom surface) are significantly larger than that of BC1 (clamped bottom surface), and the transverse and in-plane coefficients for BC3 are slightly higher than that of BC4, (3) For BC1, the peak of all the coefficients occurs when the volume fraction is approximately 0.7, while it is at approximately 0.4 for BC2, (4) double-humped curve appears for BC3 and BC4 where there is traction-free or near traction-free BCs; this was also predicted in the analytical model of [Petrov and Srinivasan (2008)] and the FE model of [Pan and Wang (2009)]. The double-humped curve is due to the fact that the strain produced consists of two components: longitudinal and flexural. In the absence of flexural strain, the maximum ME coefficient occurs at $V_f \approx 0.4$. Since the flexural strain is of opposite sign relative to the longitudinal strain, the two types of strains combine to produce suppression of the ME voltage coefficients at $V_f \approx 0.4$, and double maximum in the ME coefficients at $V_f \approx 0.15$, 0.75.

When the magnetic loading is combined with uniformly distributed mechanical stress on the upper surface as in Figure 7 (upper), we define a non-dimensional

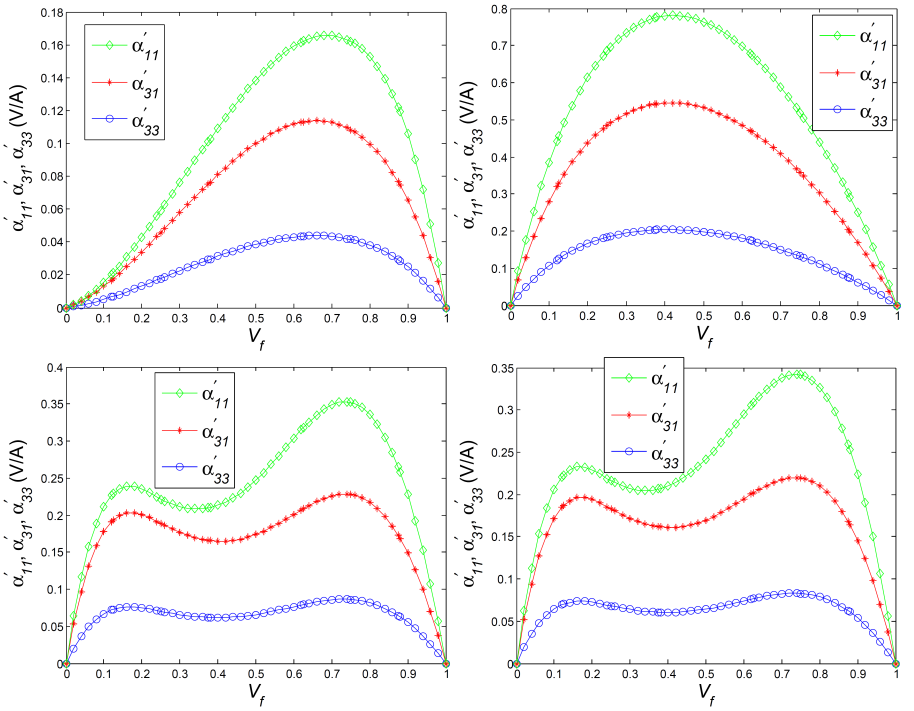

Figure 8: The three ME voltage coefficient as a function of the volume fraction for: BC1 (upper left), BC2 (upper right), BC3 (lower left), and BC4 (lower right).

quantity χ^m:

$$\chi^m = \frac{\sigma_0}{\tilde{d}\tilde{H}} \tag{98}$$

where $\tilde{d} = d_{33}$ and $\tilde{H} = \begin{cases} |\bar{H}_3| & \text{for out - of - plane mode} \\ |\bar{H}_1| & \text{for transverse and in - plane modes} \end{cases}$.

Using $V_f = 0.5$, we calculate the three ME voltage coefficients as a function of χ^m. Since the magnetic field, $\tilde{H}$, is constant, increasing χ^m is equivalent to increasing the applied load. Applying uniformly distributed stress on the top surface, the effect of varying the non-dimensional parameter χ^m on the three ME voltage coefficients for BC1 and BC2 cases is shown in Figure 9, while Figure 10 shows the effect of varying χ^m on the three ME voltage coefficients for BC3 and BC4 cases with uniformly distributed stress applied on the right surface.

It can be seen that the applied mechanical stress enhances all the ME voltage coefficients. Also note that when the stress is applied on the upper surface for BC1 and

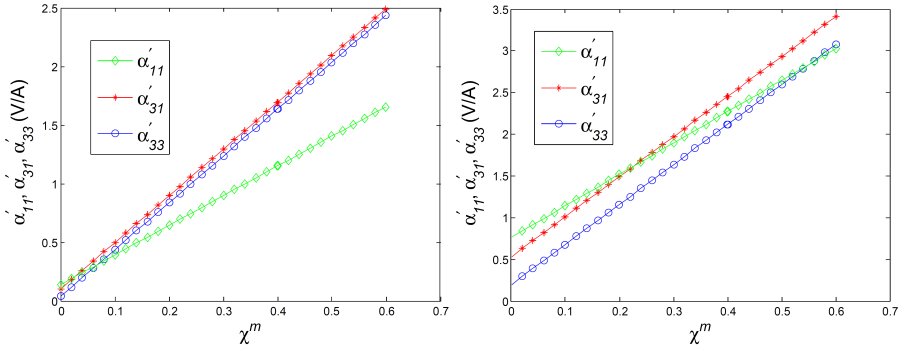

Figure 9: Effect of the non-dimensional parameter χ^m on the three ME voltage coefficients for uniformly distributed stress on the top surface with $V_f = 0.5$: (left): BC1, (right): BC2

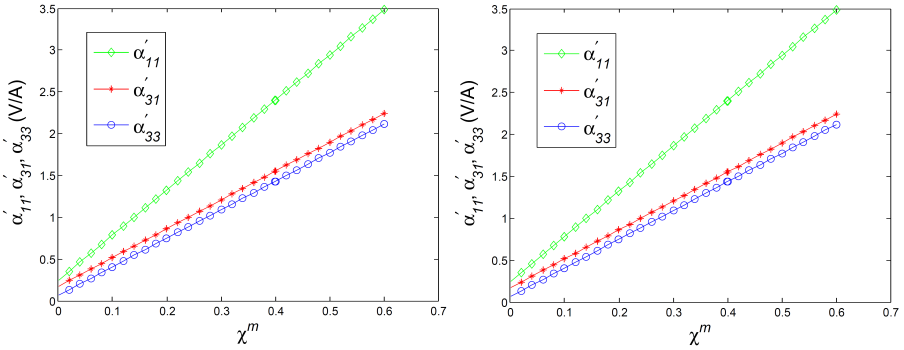

Figure 10: Effect of the non-dimensional parameter χ^m on the three ME voltage coefficients for uniformly distributed stress on the right surface with $V_f = 0.5$: (left): BC3, (right): BC4

BC2, the out-of-plane and the transverse ME coefficients are enhanced more than the in-plane coefficient (since they have larger slope) and at some values of χ^m , or equivalently σ_0, the values of the out-of-plane and transverse ME coefficients exceeds that of the in-plane coefficient. This is expected since the load is applied out-of-plane. However, with BC3 and BC4, when the uniform stress is applied on the right surface, the in-plane ME coefficient is enhanced more than the other two ME voltage coefficients. This is also expected since the load is applied in-plane.

Now we investigate the effect of subjecting the composite to bending-like loads; this is not presented in any published article. We will only consider BC3 and BC4

for these calculations. The non-dimensional parameter χ^m is defined here as:

$$\chi^m = \begin{cases} \frac{\sigma_0}{\tilde{d}\tilde{H}} \times 10^2 & \text{for } \sigma_0 \text{ in the horizontal direction} \\ \frac{P}{\tilde{d}\tilde{H}t} \times 10 & \text{for } P \text{ applied on the right surface} \\ \frac{M}{\tilde{d}\tilde{H}tL} \times 10^2 & \text{for } M \text{ applied on the right surface} \end{cases} \tag{99}$$

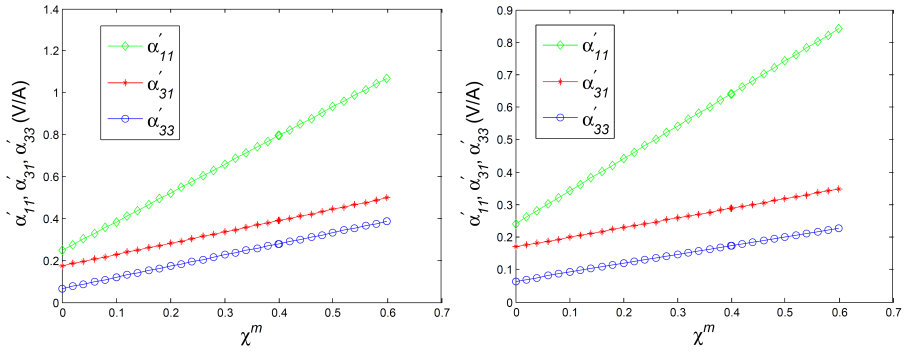

Figure 11: Effect of the non-dimensional parameter χ^m on the three ME voltage coefficients for uniformly distributed stress on the top surface with $V_f = 0.5$: (left): BC3, (right): BC4

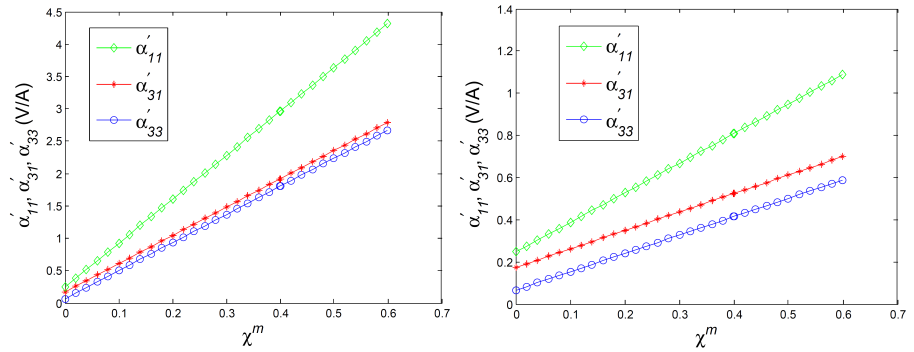

Figure 12: Effect of the non-dimensional parameter χ^m on the three ME voltage coefficients with $V_f = 0.5$ for BC3 with (left): end shear load, (right): end moment load on the right surface

Figure 11 shows the effect of varying χ^m on the ME voltage coefficients with V_f = 0.5 and uniformly distributed stress directed upwards applied on the upper surface

of the composite, while Figure 12 shows the cases of vertically upward concentrated shear force and anticlockwise bending moment applied on the right surface. Figure 12 is only for BC3 since the results of BC4 are very similar to that of BC3 for these cases.

The applied bending mechanical loads, which are calculated from eq. (99), highly enhance the ME voltage coefficients even more than the tensile loads in Figure 9 and Figure 10 (note the factors 10 and 10^2 in calculating the applied bending loads in eq. (99) to recognize that Figure 11 and Figure 12 show the trend for only small applied bending loads). It can also be seen that the in-plane ME voltage coefficient increases with larger slope.

In all the previous calculations, care was taken not to allow the generated stresses in the composite exceed the material yield strength (which is in the range of 32MPa for PZT-5A). No Experimental results are published with combined mechanical and magnetic loadings. Experimental testing is required to verify these results.

5.3 Bi-layered piezoelectric-piezomagnetic composites with functionally-graded layers

In this set of computational experiments we make one of the two layers functionally graded and show the effect of the different grading functions on the ME voltage coefficients. The functions used to grade all the material properties of the piezoelectric and piezomagnetic layers in x_3-direction are:

$$\begin{aligned} f_{ij}(\mathbf{x}) &= f_{ij}^0 \exp\left[n_E\left(\frac{x_3 - x_{3l(PE)}}{t_e}\right)\right] \quad \text{for the PE layer} \\ f_{ij}(\mathbf{x}) &= f_{ij}^0 \exp\left[n_M\left(\frac{x_3 - x_{3l(PM)}}{t_m}\right)\right] \quad \text{for the PM layer} \end{aligned} \tag{100}$$

where $f_{ij}(\mathbf{x})$ is the material property at point $\mathbf{x}$, f_{ij}^0 is the material properties of PZT-5A or $CoFe_2O_4$, $x_{3l(PE)}$ and $x_{3l(PM)}$ are the x_3-coordinates of the lower surface of the PE and PM layers respectively. In our analysis, we use different values of the exponents n_E and n_M. Note that if n_E or n_M is positive, then the values of the material properties are getting larger as we go from the lower to the upper surfaces of the PE or PM layer (the values at the upper surface is 2.7183 times that at the lower surface when n_E or n_M= 1), while if n_E or n_M is negative, then the material is getting softer as we go from the lower to the upper surfaces.

For the clamped BC case (BC1), and equal thicknesses of both layers (V_f = 0.5), the effect of n_E and n_M on the three ME voltage coefficients is shown in Figure 13.

It can be seen that as n_E decreases, and n_M increases, the out-of-plane and transverse ME coefficients increase. The largest value of α'_{33} is obtained when $n_E = -1$ and $n_M = 1$. This corresponds to the case where the PE material has lower strength

at the top surface of the PE layer, with the material properties at the top surface equal to 0.3679 times that at the bottom surface, and the PM material has higher strength at the top surface of the PM layer, with the material properties at the top surface equal to 2.7183 times that at the bottom surface. The in-plane ME coefficient increases as both n_E and n_M increase. However the improvement in all of the ME coefficients is not highly significant.

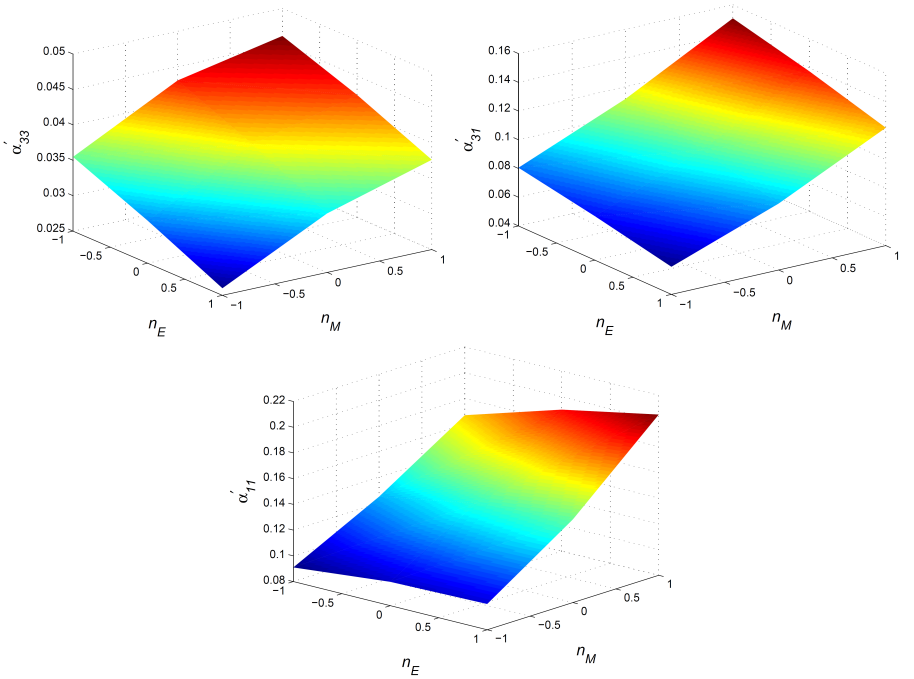

Figure 13: Clamped BC (BC1) case with $V_f = 0.5$: the effect of the exponents n_E and n_M on the ME voltage coefficients (upper left) α'_{33}, (upper right): α'_{31}, (lower) α'_{11}

The results of BC2 are presented in Figure 14. The same trends can be observed but all the ME coefficients are higher as was discussed in the previous section.

5.4 Single-layer functionally graded magneto-electro-elastic material

In this set of numerical experiments we consider only one functionally graded layer whose properties are changed from pure piezomagnetic at the bottom surface to pure piezoelectric at the top surface. Figure 15 shows the electric and magnetic BCs used to simulate these three modes of the ME voltage coefficients for this type

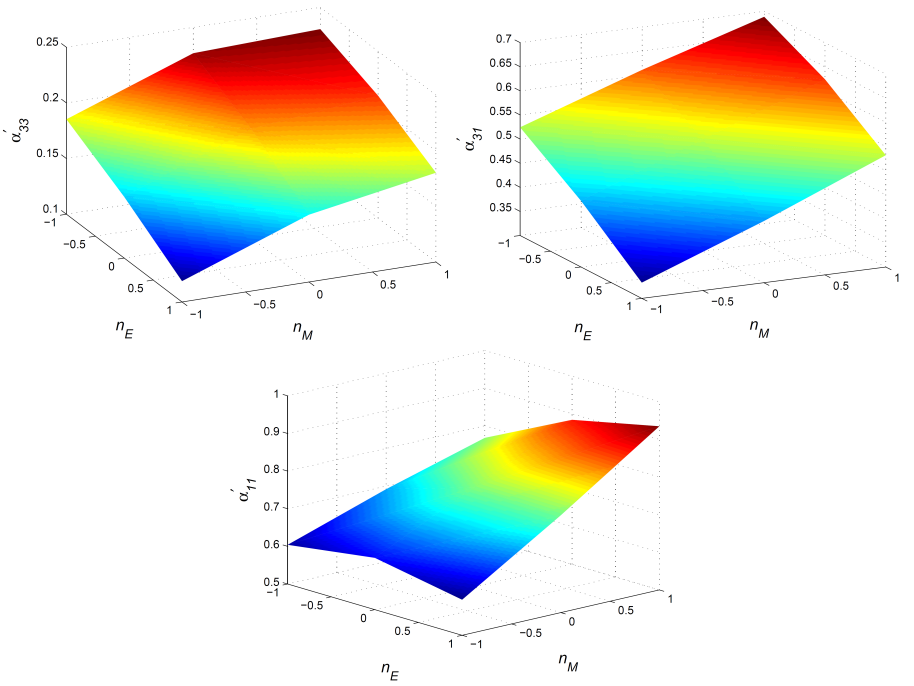

Figure 14: BC2 case with $V_f = 0.5$: the effect of the exponents n_E and n_M on the ME voltage coefficients (upper left) α'_{33}, (upper right): α'_{31}, (lower) α'_{11}

of composites. $\bar{\Psi}_{low}$ in eq. (95) is calculated as: $\bar{\Psi}_{low} = \bar{H}_3 t$ A. The thickness of the composite to be used in the numerical simulations is 2 mm while the length is still 16 mm. Magnetic field of -100 A/m is to be applied.

The material properties are graded in x_3-direction according to the following relation:

$$f_{ij}(\mathbf{x}) = f_{ij}^B + (f_{ij}^T - f_{ij}^B)\left(\frac{x_3 - x_{3l}}{t}\right)^n \tag{101}$$

where $f_{ij}(\mathbf{x})$ is the material property at the point $\mathbf{x}$, f_{ij}^B, f_{ij}^T are the material properties of $CoFe_2O_4$ and PZT-5A respectively, x_{3l} is the x_3-coordinate of the lower surface of the composite.

The effect of varying the exponent n on the out-of-plane and transverse ME voltage coefficients for BC1 and BC2 is presented in Figure 16.

One can observe that the maximum ME voltage coefficient values are at the exponent value of about 0.5. The transverse ME coefficient α'_{31} is significantly larger

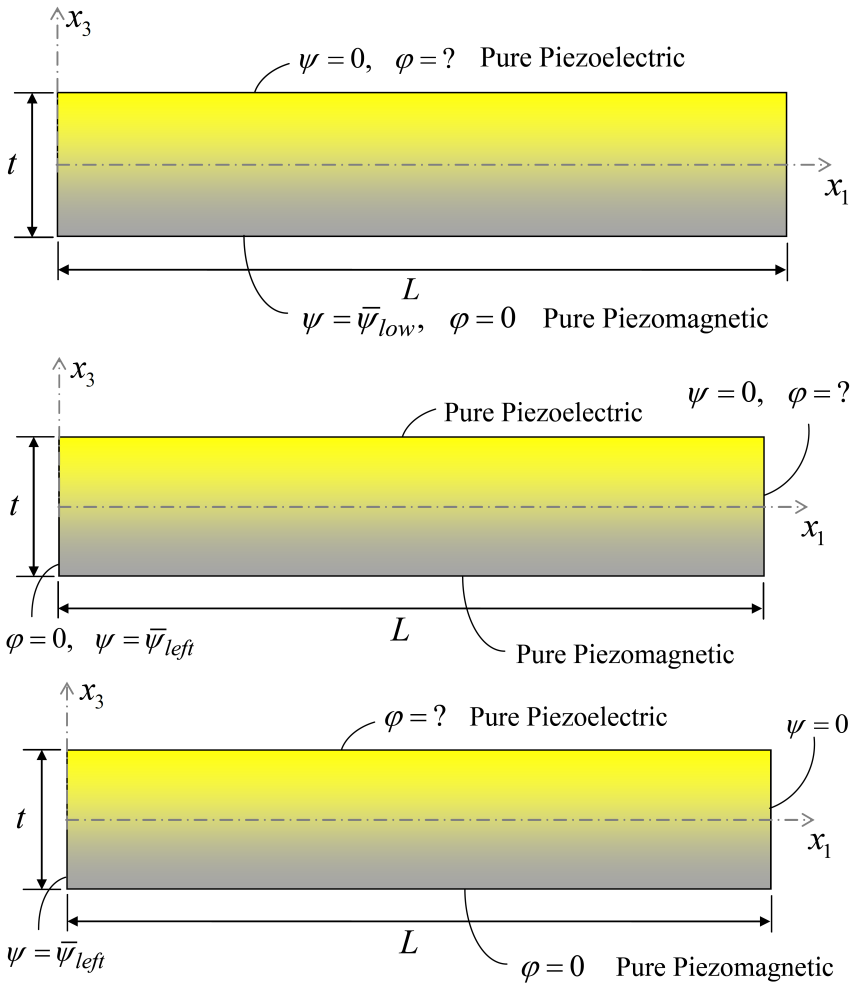

Figure 15: The electric and magnetic BCs for the three modes of the ME voltage coefficient in the single layer functionally graded magneto-electro-elastic material: (upper) out-of-plane, (middle) transverse, (lower) in-plane

than the out-of-plane ME coefficient α'_{33} (about 5 times). We can also see that different mechanical boundary conditions on the bottom surface of the FGM plate have only slight influence on the homogenized ME coefficients. The peak value of the out-of-plane ME coefficient is slightly larger for the clamped condition (BC1) than in the fixed BC case (BC2).

Similar to the case of the bi-layered PE-PM composites with pure constituents pre-

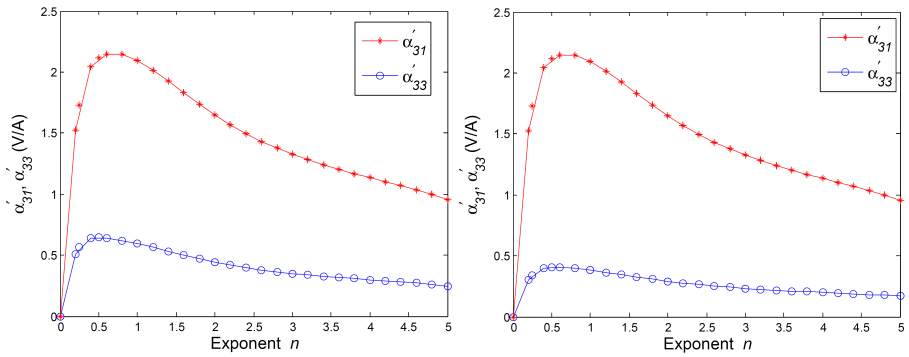

Figure 16: Effect of the exponent n on the out-of-plane and transverse ME voltage coefficients for the clamped BC1 case (left) and fixed BC2 case (right)

sented in subsection 5.2, combining mechanical loads with the applied magnetic loads enhances the ME voltage coefficients of PE-PM composites with functionally graded layers and single-layered functionally graded MEE materials.

6 Conclusions

HMFEM-C element developed in this paper based on the primal variational principle for modeling MEE materials proved to be significantly more accurate than the primal finite element. Using a validated computer code for modeling MEE materials, bi-layer PE-PM composites are analyzed and it was shown that: (1) for all the considered BCs, the in-plane ME voltage coefficient α'_{11} is the largest, followed by the transverse, α'_{31}, then the out-of-plane ME voltage coefficient, α'_{33}, (2) all the three ME voltage coefficients for BC2 (bottom surface fixed in the vertical direction only) are significantly larger than that of BC1 (totally clamped bottom surface), (3) for BC1, the peak of all the coefficients occurs when the volume fraction is approximately 0.7, while it is at approximately 0.4 for BC2. Double-humped curve appears for BC3 and BC4 where there is traction-free or near traction-free BCs, (4) combining the applied magnetic loads with mechanical loads generally enhances the ME voltage coefficients, (5) bending loads can highly enhance the ME voltage coefficients even more than tensile loads.

Using node-wise material properties in the finite element is more suitable in modeling FGM than the element-wise material properties used with the conventional finite elements. Analyzing bi-layered PE-PM composites with the material properties, of one or both of the layers, graded exponentially, it was concluded that grading the PE layer so that its properties are weaker on its top surface while grad-

ing the PM layer so that its properties are stronger on its top surface enhances the out-of-plane and transverse modes, while we need stronger properties on the top surface of the PE and PM layers in order to get the highest in-plane ME voltage coefficient.

It follows from the numerical analyses of single-layer functionally graded magneto-electro-elastic material that optimal gradation is for exponent $n = 0.5$ in power-law gradient composites with ferromagnetic and ferroelectric phases. It corresponds to the case where there is a significant material gradation close to the bottom surface with pure piezomagnetic properties.

The electric potential in the PE layer is induced by the magnetic potential in the PM layer. The induced electric field is not uniform on the top surface of the PE layer. Therefore, the magnetoelectric coefficient is also not uniform. The presented ME voltage coefficients correspond to the average value of the induced electric potential at the top of the PE layer. Some results considered in the paper need to be experimentally verified.

Acknowledgement: This work was supported in part by the Vehicle Technology Division of the Army Research Labs, under a collaborative research agreement with University of California, Irvine (UCI), and in part by the Word Class University (WCU) program through the National Research Foundation of Korea, funded by the Ministry of Education, Science and Technology (Grant no.: R33-10049). The authors also acknowledge the support by the Slovak Science and Technology Assistance Agency registered under number APVV-0014-10.

References

Atluri, S. N. (1975): On hybrid finite element models in solid mechanics. In Vichnevetsky, R. (ed.): *Advances in Computer Methods for Partial Differential Equations*, Proceedings of the international symposium, International Organization, AICA, pp. 346–356.

Atluri, S. N.; Tong, P.; Murakawa, H. (1983): Recent studies in hybrid and mixed finite element methods in mechanics. In Atluri, S.N.; Gallagher, R.H.; Zienkiewicz, O.C. (eds.): *Hybrid and Mixed Finite Element Methods*, pp. 51–71.

Babuska, I. (1973): The finite element method with Lagrangian multipliers. *Numerische Mathematik*, vol. 20, no. 3, pp. 179–192.

Benjeddou, A. (2000): Advances in piezoelectric finite element modeling of adaptive structural elements: a survey. *Computers and Structures*, vol. 76, pp. 347-363.

Bichurin, M.I.; Petrov, V.M.; Srinivasan, G. (2003): Theory of low-frequency magnetoelectric coupling in magnetostrictive-piezoelectric bilayers. *Physical Re-*

view B, vol. 68, 054402.

Bishay, P. L.; Atluri, S. N. (2012): High-Performance 3D Hybrid/Mixed, and Simple 3D Voronoi Cell Finite Elements, for Macro- & Micro-mechanical Modeling of Solids, Without Using Multi-field Variational Principles. *CMES: Computer Modeling in Engineering & Sciences*, vol. 84, no. 1, pp. 41-98.

Brezzi, F. (1974): On the existence, uniqueness and approximation of saddle-point problems arising from Lagrangian multipliers. *Revue Française D'automatique, Informatique, Recherche Opérationnelle, Analyse Numérique*, vol. 8, no. 2, pp. 129–151.

Carbonari, R. C.; Silva, E. C. N.; Paulino, G. H. (2007): Topology optimization design of functionally graded bimorph-type piezoelectric actuators. *Smart Mat. Struct.*, vol. 16, pp. 2605-2620.

Carbonari, R. C.; Silva, E. C. N.; Paulino, G. H. (2009): Multi-actuated functionally graded piezoelectric micro-tools design: A multiphysics topology optimizatoin approach. *Int. J. Numer. Meth. Eng.*, vol. 77, pp. 301-336.

Carbonari, R. C.; Paulino, G. H.; Silva, E. C. N. (2010): Integral piezoactuator system with optimum placement of functionally graded material - A topology optimization paradigm. *J. Intel. Mat. Systems Structures*, vol. 21, pp.1653-1668.

Chang, C; Carman, G. P. (2008): Analytically Evaluating the Properties and Performance of Layered Magnetoelectric Composites. *J. Intell. Mater. Syst. Struct.*, vol. 19, pp.1271-1280.

Cheong, S.; Mostovoy, M (2007): Multiferroics: a magnetic twist for ferroelectricity. *Nature Mater.*, vol. 6, pp. 13-20.

Dong, L.; Atluri, S. N. (2011): A simple procedure to develop efficient & stable hybrid/mixed elements, and Voronoi cell finite elements for macro- & micromechanics. *CMC: Computers, Materials & Continua*, vol. 24, no. 1, pp. 61–104.

Dunn, M.L. (1993): Micromechanics of coupled electroelastic composites: effective thermal expansion and pyroelectric coefficients. *Journal of Applied Physics*, vol. 73, pp. 5131-5140.

Eerenstein, W.; Mathur, N.D.; Scott, J.F. (2006): Multiferroic and magnetoelectric materials. *Nature*, vol. 442, pp. 759-765.

Feng, W.J.; Su, R.K.L. (2006): Dynamic internal crack problem of a functionally graded magneto-electro-elastic strip. *Int. J. Solids Structures*, vol. 43, pp. 5196-5216.

Ghandi, K.; Hagood, N. W. (1997): A hybrid finite element model for phase transitions in nonlinear electro-mechanically coupled material. In Varadan, V. V.; Chandra, J. (eds.): *Smart Structures and Materials 1997: Mathematics and Control*

in Smart Structures. Proceedings of SPIE 3039, pp. 97-112.

Heyliger, P.; Ramirez, F.; Pan, E. (2004): Two-dimensional static fields in magnetoelectroelastic laminates. *J. Intelligent Materials Systems and Structures*, vol. 15, pp. 689-709.

Heyliger, P. R.; Ramirez, G.; Saravanos, D. A. (1994): Coupled discrete-layer finite elements for laminated piezoelectric plates. *Commun. Numer.Methods Engrg.*, vol. 10, pp. 971-981.

Hill, N. A. (2000): Why are there so few magnetic ferroelectrics? *J. Phys. Chem. B*, vol. 104, pp. 6694–6709.

Hossack, J. A.; Hayward, G. (1991): Finite-element analysis of 1-3 composite transducers. *IEEE Trans. Ultrasonics, Ferroelectrics & Frequency Control*, vol. 38, pp. 618-627.

Hwang, W. S.; Park, H. C. (1993): Finite element modeling of piezoelectric sensors and actuators. *AIAA J.*, vol. 31, pp. 930-937.

Jiang A.; Ding H. (2004): Analytical Solutions to Magneto-electro-elastic Beams. *Structural Engineering and Mechanics*, vol.18, pp.195–209.

Kagawa, Y.; Yarnahuchi, T. (1974): Finite element simulation of two-dimensional electromechanical resonators. *IEEE Trans. Sonics Ultrason.*, vol. SU-21, pp. 275-283.

Khomskii, D. I. (2001): Magnetism and ferroelectricity: why do they so seldom coexist? *Bull. Am. Phys. Soc. C* 21.002.

Kim, J.; Varadan, V.V.; Varandan, V.K. (1997): Finite element modelling of structures including piezoelectric active devices. *Inter.J.Numer.Methods Engrg.*, vol. 40, pp. 817-832.

Laletin, V.M.; Petrov, V.M.; Tuskov, D.S.; Srinivasan, G. (2008): Frequency dependence of the magnetoelectric effect in ceramic composites based on lead zirconate titanate and nickel ferrite. *Tech. Phys. Lett.*, vol. 34, pp. 83-89.

Lerch, R. (1990): Simulation of piezoelectric devices by two- and three-dimensional finite elements. *IEEE Trans. Ultrasonics, Ferroelectrics & Frequency Control*, vol. 37, pp. 233-247.

Lines, M. E.; Glass, A. M. (2001): *Principles and Applications of Ferroelectrics and Related Materials*, Oxford Univ. Press, Oxford.

Miyamoto, Y.; Kaysser, W. A.; Rabin, B. H.; Kawasaki, A.; Ford, R. G. (1999): *Functionally graded materials: Design, Processing and Applications*. Kluwer Academic Publishers, Boston.

Naillon, M.; Coursant, R.; Besnier, F. (1983): Analysis of piezoelectric structures

by a finite element method. *Acta Electronica*, vol. 25, pp. 341-362.

Nan, C.W. (1994): Magnetoelectric effect in composites of piezoelectric and piezomagnetic phases. *Phys. Rev. B*, vol. 50, pp. 6082-6088.

Nan, C.W.; Bichurin, M.I.; Dong, S.X.; Viehland, D. (2008): Multiferroic magnetoelectric composites: Historical perspective, status, and future directions. *Journal of Applied Physics,* 103,031101.

Pan, E.; Wang, R. (2009): Effects of geometric size and mechanical boundary conditions on magnetoelectric coupling in multiferroic composites. *Journal of Physics D: Applied Physics,* vol. 42, 245503 (7pp).

Pian, T. H. H.; Chen, D. (1983): On the suppression of zero energy deformation modes. *International Journal for Numerical Methods in Engineering*, vol. 19, issue 12, pp. 1741–1752.

Punch, E. F.; Atluri, S. N. (1984): Development and testing of stable, invariant, isoparametric curvilinear 2- and 3-D hybrid-stress elements. *Computer Methods in Applied Mechanics and Engineering*, vol. 47, no. 3, pp. 331–356.

Rubinstein, R.; Punch, E. F.; Atluri, S. N. (1984): An analysis of, and remedies for, kinematic modes in hybrid-stress finite elements: selection of stable, invariant stress fields. *Computer Methods in Applied Mechanics and Engineering*, vol. 38, no. 1, pp. 63–92.

Ryu, J.; Priya, S.; Uchino, K.; Kim, H.E. (2002): Magnetoelectric effect in composites of magnetostrictive and piezoelectric materials. *J. Electroceramics,* vol. 8, pp. 107-119.

Saravanos, D. A.; Heyliger, P. R.; Hopkins, D.H. (1997): Layerwise mechanics and finite element for the dynamic analysis of piezoelectric composite plates, *Inter.J.Solids & Structures*, vol. 34, pp. 359-378.

Schmid, H. (1994): Multi-ferroic magnetoelectrics. *Ferroelectrics*, vol. 162, pp. 317–338.

Shastry, S.; Srinivasan, G.; Bichurin, M.I.; Petrov, V.M.; Tatarenko, A.S. (2004): Microwave magnetoelectric effects in single crystal bilayers of yttrium iron garnet and lead magnesium niobate-lead titanate. *Phys. Rev. B*, vol. 70, 064416.

Shaulov, A.A.; Smith, W.A.; Ting, R.Y. (1989): Modified-lead-titanate/polymer composites for hydrophone applications. *Ferroelectrics*, vol. 93, pp. 177-182.

Sladek J.; Sladek V.; Krahulec, S.; Pan, E. (2012a): Enhancement of the magnetoelectric coefficient in functionally graded multiferroic composites. *Journal of Intelligent Material Systems and Structures,* vol.23, pp. 1644-1653.

Sladek J.; Sladek V.; Krahulec, S.; Wünsche M.; Zhang, C. (2012b): MLPG analysis of layered composites with piezoelectric and piezomagnetic phases. *CMC:*

Computers, Materials & Continua, vol. 29, pp. 75-101.

Smith, W.A.; Shaulov, A.A. (1985): Tailoring the properties of composite piezoelectric materials for medical ultrasonic transducers. *IEEE Ultrasonic Symposium*, vol. 2, pp. 642-647.

Sze, K. Y.; Pan, Y. S. (1999): Hybrid finite element models for piezoelectric materials. *Journal of Sound and Vibration*, vol. 226 (3), pp. 519-547.

Tang, L.; Chen, W.; Liu, Y. (1984): Formulation of quasi-conforming element and Hu-Washizu principle. *Computers & Structures*, vol. 19, issue 1-2, pp. 247–250.

Tzou H. S.; Tseng, C. I. (1990): Distributed piezoelectric sensor/actuator design for dynamic measurement/ control of distributed parameter systems: a finite element approach. *J. Sound & Vibration*, vol. 138, pp. 17-34.

Tzou, H.S. (1993): *Piezoelectric Shells: Distributed Sensing and Control of Continua*, Kluwer Academic Publishers, Dordrecht.

Tzou, H. S.; Ye, R. (1996): Analysis of piezoelectric structures with laminated piezoelectric triangle shell element. *AIAA J.*, vol. 34, pp. 110-115.

Van Aken, B. B.; Palstra, T. T. M.; Filippetti, A.; Spaldin, N. A. (2004): The origin of ferroelectricity in magnetoelectric $YMnO_3$. *Nature Mater.*, vol. 3, pp. 164–170.

Wang, Y.; Yu, H.; Zheng, M.; Wan, J.G.; Zhang, M.F.; Liu, J.M.; Nan, C.W. (2005): Numerical modeling of the magnetoelectric effect in magnetostrictive piezoelectric bilayer. *Applied Physics A*, vol. 81, pp. 1197-1202.

Zhai, J.Y.; Cai, N.; Shi, Z.; Lin, Y.H.; Nan, C.W. (2004): Coupled magnetoelectric properties of laminated $PbZr_{0.53}Ti_{0.47}O_3/NiFe_2O_4$ ceramics. *J. Appl. Phys.*, vol. 95, p. 5685.